HOCHSCHULE COBURG

STUDIENGANG

MASCHINENBAU

B A C H E L O R A R B E I T

Muhammad Afif Bin Zulkifli

Evaluation of known slip factor models using computational fluid dynamics (CFD)

Bachelorarbeit

zur Erlangung des akademischen Grades eines

Bachelor of Engineering (B.Eng.)

HOCHSCHULE COBURG

Ausgabetermin:	24.11.2016
Abgabetermin:	28.02.2017
Autor:	Muhammad Afif Bin Zulkifli (Mnr: 00271012)
Hochschule:	Hochschule für angewandte Wissenschaften Coburg Studiengang Maschinenbau Friedrich-Streib-Str. 2 96450 Coburg
Firmenbetreuer:	-
Erstprüfer:	Prof. Dr. Philipp Epple

1 Declaration of Autorship

I assure that I have written the present work independently and without any means other than those indicated. The ideas taken directly or indirectly from other sources are marked as such.

Location, Time: Coburg, the 27.02.2017 Signature: 

Muhammad Afif Bin Zulkifli

2 Foreword/ Acknowledgement

Firstly, I want to thank God for the plans and help that He had made for and given to me. The possibility and the writing of this bachelor thesis could also not have been made possible without the people who have helped me in all shapes and forms especially my family members, my mother Adzlinda I. which have given me the support I needed along my journey, my friends throughout Germany and Malaysia especially Faid F., Seif B., Samed S., and Sercan K. who have been with me throughout my studies, my dearest teachers and professors particularly Prof. Dr. Philipp Epple who has taught me a lot in the dream engineering field, fluid mechanics and turbomachinery which I would might not knew before, as well as my scholar MARA who has helped tremendously financially for me to experience life overseas and becoming and engineer. Thank you.

3 Short summary/ Abstract

English:

Evaluation of known Slip Factor models using computational fluid dynamics (CFD)

The latest state of the art Slip Factor models by Wiesner, Pfleiderer and modified variants by Guelich and Aungier should be reviewed and possibly further extended with other parameters with the help of sensitivity analysis.

By using the optimization software CFturbo as geometry generator and a commercial CFD program STAR CCM+, radial and semi-axial pumps or compressors should be examined in a process to determine the aerodynamic and hydraulic behaviors.

Deutsch:

Evaluierung etablierter Minderleistungsmodelle mittels numerische Strömungssimulation

Stand der Technik sind Minderleistungsmodelle nach Wiesner, Pfleiderer und modifizierte Varianten davon nach Gülich und Aungier. Mithilfe einer Sensitivitätsanalyse sollen diese Modelle überprüft und ggf. durch weitere Parameter erweitert werden. Dazu sollen radiale und halb-axiale Pumpen oder Verdichter in einem Prozess untersucht werden, in dem eine Optimierungssoftware CFturbo als Geometriegenerator ansteuert und ein kommerzielles CFD-Programm Star CCM+ zur Ermittlung des aerodynamischen bzw. hydraulischen Verhaltens verwendet wird.

4 Table of contents

5 Operation of a centrifugal pump

Pumps are used to increase pressure of liquids. Centrifugal pumps are the most preferred pump in the hydraulic industry. Centrifugal pump operates by sucking water from the eye of the impeller and imparts centrifugal force to the water by rotation of the impeller. The fluid which then flows from the impeller eye between the impeller blades will be accelerated and have increased velocity. Per Bernoulli's principle, an increased velocity of fluid flow causes a decrease in pressure. This lower pressure is what causes the fluid to be sucked into the impeller eye.

After the fluid leaves the impeller, a special casing surrounding the sides of the impeller called a volute helps to decrease the velocity of the fluid and thereby increasing the exit pressure. The volute casing is specially designed to have an increasing surface area to accommodate the increasing amount of fluid leaving the impeller along the circumference of the impeller.

Figure 1: A centrifugal pump [7]

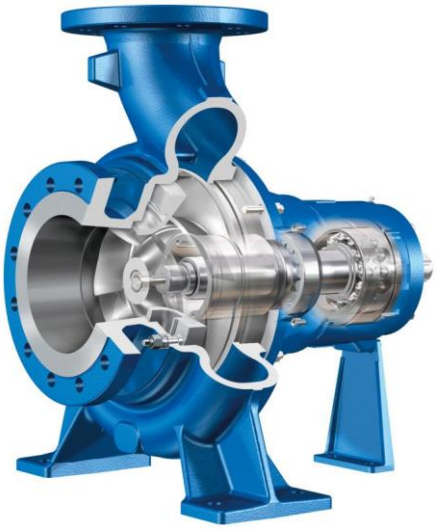

Figure 2: An impeller inside a centrifugal pump [7]

6 Impeller types and characteristics

In centrifugal pumps, an impeller is the rotating component (also called rotor) with built in blades or vanes. An impeller is typically made from iron, steel, bronze, brass, aluminum or plastic.

6.1 Types of impellers

Impellers can be divided into three types:

6.1.1 Open impeller

Figure 3: Open impeller [4]

Open impeller has a series of vanes attached to the central hub without sidewalls or shroud. The hub mounts directly to the shaft. Open impellers are structurally weaker than its counter parts so they are typically being in service as small-diameter, inexpensive pumps. This design causes the blades to experience more wear compared to other impeller types.

Generally, open impellers are inefficient, but the efficiency can be maintained through clearance adjustments. Because of the open design, it is cheaper to build and it is less likely to get clogged. It also has a greater range of specific speeds. Thus, it is more favored in handling more viscous fluids and fluid with solid suspensions.

6.1.2 Semi open impeller

Figure 4: Semi open impeller [4]

Semi open impellers have either a hub at the front or at the back of the impeller each with its own advantages and disadvantages. Because of the one hub surface, semi open impellers

experience heavy axial thrust as the fluid pressure builds upon it. Thrust balancing technique is needed to reduce the stress on the bearings but at the same time increases power consumption, lowering the efficiency and increases leakage losses.

But semi open impeller benefits in that it allows suspensions that would normally clog a closed impeller to pass. It also has reduced leakage loss compared to open impellers because the fluid has only one leakage path which is over the blade.

6.1.3 Closed impeller

Figure 5: Closed impeller [5]

The blades are sandwiched between the top cover called a shroud and the bottom wall called the hub. Wear ring is mounted to restrict the amount of fluid discharge that recirculates back to the suction side of impeller. It is the most popular impeller type in the industry since they can deal with extremely volatile and explosive fluids because the close clearance of wear rings can compensate for shaft displacement from centerline. Closed impellers are very efficient but loses efficiency over time as wear ring clearance increases. When the wear ring experiences too much clearance, it must be replaced.

During maintenance process, closed impeller must be disassembled from the pump to check the status of the wear rings. In open impeller, disassembly is not required. Other internal parts are also hidden so it is very difficult to inspect for damages. It is the most popular impeller type in the industry since they can deal with extremely volatile and explosive fluids because the close clearance of the wear rings can compensate for shaft displacement from the centerline.

Per DIN 24250 [1], the distinction can be made between clockwise and counter-clockwise impellers by viewing in inlet flow direction.

6.2 Direction of through flow of impeller

Depending on the through flow direction, impellers can be classified into the following four types:

6.2.1 Radial Impeller

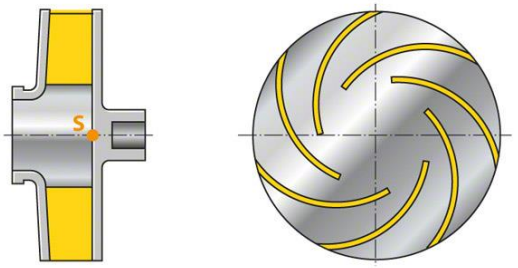

Figure 7: Radial impeller with purely radial vanes, shroud removed [4]

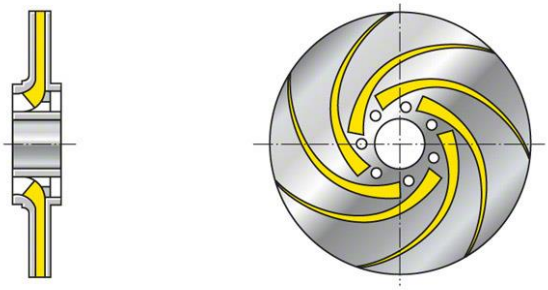

Figure 6: Radial impeller with vanes extending into suction eye, shroud removed [4]

An Impeller is called a radial impeller when the flow leaves the impeller radially outwards from the axis of rotation, perpendicular to the pump shaft. Mechanical energy from the vanes imparts centrifugal energy to the fluid by deflecting the flow direction at the impeller vanes.

6.2.2 Mixed flow Impeller

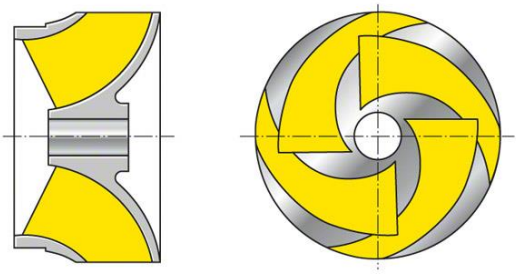

Figure 9: Mixed-flow impeller (diagonal impeller), shroud removed [4]

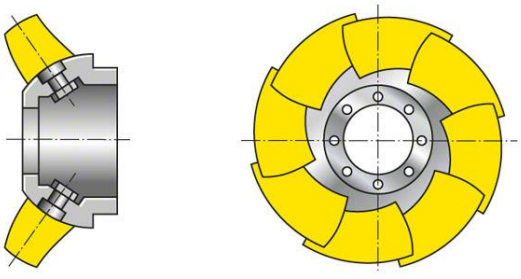

Figure 8: Mixed-flow Impeller (Mixed flow propeller) [4]

Mixed flow impellers are also called semi-axial impellers. Mixed flow impellers live inside centrifugal pumps and covers the transition range between radial impellers and axial impellers. Mixed flow Impeller are used in mixed flow pumps. Because mixed flow pumps have a wide range of operation, the build can be either one of two types. Impellers

of mixed flow pumps with low specific speed are assembled with a volute casing while impellers with high specific speed are combined with a diffuser and tubular casing.

6.2.3 Axial flow Impeller

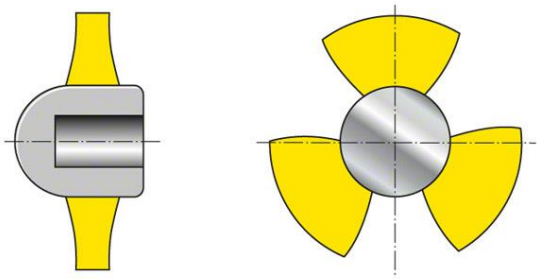

Figure 10: Axial impeller (Axial propeller) [4]

An axial flow impeller is often called propeller. An axial flow impeller is a component of axial flow pump. The propeller can be driven directly by a sealed motor which resides in the pipe or a motor mounted to the pipe from the outside or at right angle by a right-angle drive shaft that pierces the pipe. The change of radius of flow between the suction side (entry) and the discharge side (exit) of the pump is very little, hence the term axial is used.

6.2.4 Peripheral Impeller

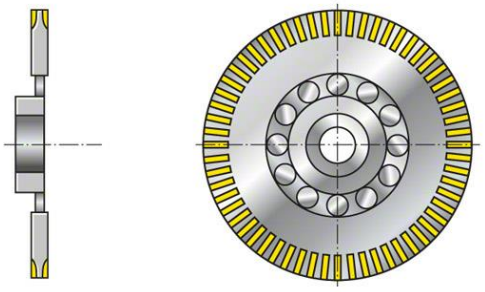

Figure 11: Peripheral impeller [4]

Peripheral Impellers are special impellers that have small double-flow impeller vanes arranged at its periphery. Peripheral impellers are used in peripheral pumps and functions as a displacement pump. Peripheral pumps lie between displacement pump and centrifugal pump because of the way medium is pumped into a peripheral channel. Unlike typical centrifugal pumps, the characteristic curve is a straight line with

maximum heads at low flow rate and low heads at peak flow. Because of the narrow column, it is not suitable for abrasive fluids.

7 Vector representation of velocities

7.1 Defining coordinate systems

Turbomachines are commonly used with a natural coordinate system. This is because the rotating motion of the blades of the rotor and the stationary blades of the stator are arranged around a common axis. The coordinate system has the axis r for radius component, u for tangential component, and x for axial component. In short, the flow in a turbomachine has three components which vary in direction. To simplify flow representation, flow is usually assumed to not vary in the tangential direction.

The meridional velocity is defined as the velocity on the axi-symmetric stream surface:

$$c_m = \sqrt{c_r^2 + c_x^2}$$

where

c_m = meridional velocity

c_r = radial velocity

c_x = axial velocity

The total flow velocity or absolute velocity is made up of the vector sum of the meridional velocity and the tangential velocity c_θ:

$$c = \sqrt{c_m^2 + c_\theta^2} = \sqrt{c_r^2 + c_x^2 + c_\theta^2}$$

For a **purely axial flow**, the radius of the flow path is constant therefore the radial flow velocity will be zero. This means that for a purely radial flow is:

$$c_m = c_x$$

and

$$c = \sqrt{c_x^2 + c_\theta^2}$$

As for **purely radial flow**, the axial flow path is constant therefore the axial flow velocity will be zero. Thus, for a purely radial flow, is:

$$c_m = c_r$$

and

$$c = \sqrt{c_r^2 + c_\theta^2}$$

The angle between the flow direction and meridional direction is called the tangential angle or more commonly known as swirl angle.

$$\propto = \tan^{-1}\left(\frac{c_\theta}{c_m}\right)$$

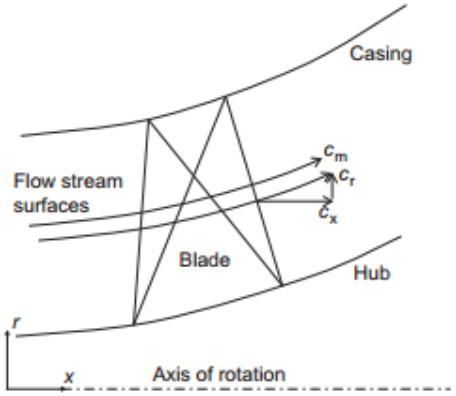

Figure 14: Meridional view (side view) [8]

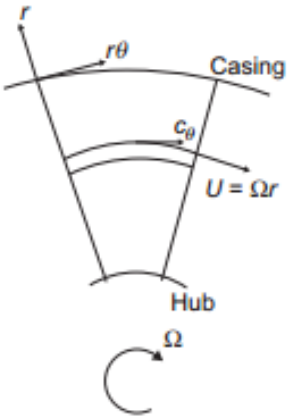

Figure 13: Axial view [8]

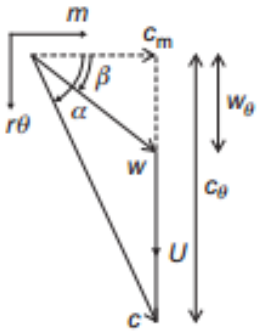

Figure 12: View looking down onto stream surface [8]

7.2 Relative velocities

Consider the flow in the turbomachine. The velocity of the rotor will be called the frame velocity or tangential velocity and be labelled as $\vec{U}$. The velocity of the fluid will then be called the absolute velocity and labelled as $\vec{c}$. From the perspective of an outside observer, the absolute velocity is clearly the velocity of the fluid but the velocity experienced by the fluid inside the rotor relative to the rotor will be different. This velocity is called the relative velocity and it has the symbol $\vec{w}$.

Understanding relative velocities in turbomachines are important as it helps in flow-field analysis within rotating blades. This process is performed in a frame of reference relative to

the blades where the flow appears as if they are steady when in fact in the absolute frame of reference, the flow would be unsteady. Steady flow means that the velocity at one point in the coordinate does not change with time.

In mathematical form, the relationship between the velocities are:

$$\vec{w} = \vec{c} - \vec{U}$$

Where

$\vec{w}$ = relative velocity

$\vec{c}$ = absolute velocity

$\vec{U}$ = tangential velocity

with rotating frame of reference

$$\vec{U} = r\Omega$$

with

r = defined radius

Ω = angular velocity

The relative velocity is the vector subtraction of tangential velocity from absolute velocity. Because the blade velocity is only in tangential direction, therefore the relative velocity components can be written as:

from:

$$\vec{w}_\theta = \vec{c}_\theta - \vec{U}_\theta$$

$$\vec{w}_r = \vec{c}_r - \vec{U}_r$$

$$\vec{w}_x = \vec{c}_x - \vec{U}_x$$

to:

$$\vec{w}_\theta = \vec{c}_\theta - \vec{U}_\theta$$

$$\vec{w}_r = \vec{c}_r$$

$$\vec{w}_x = \vec{c}_x$$

This is valid for all turbomachines whether it is an axial flow machine, radial flow machine or mixed-flow machine.

Relative flow angle β is the name given for the angle between relative flow direction and the meridional direction.

$$\beta = \tan^{-1}\left(\frac{w_\Theta}{w_m}\right) = \tan^{-1}\left(\frac{w_\Theta}{c_m}\right)$$

Thus,

$$\tan\beta = \tan\propto - \frac{U}{c_m}$$

7.3 Vector sign convention

In many turbomachinery literature, positive values for tangential velocities are defined by the direction of rotation of rotor. Tangential velocities that are in the direction of rotation is considered positive value while tangential velocities that are in the opposite direction of rotation is considered negative value. This means that it is possible to have negative value

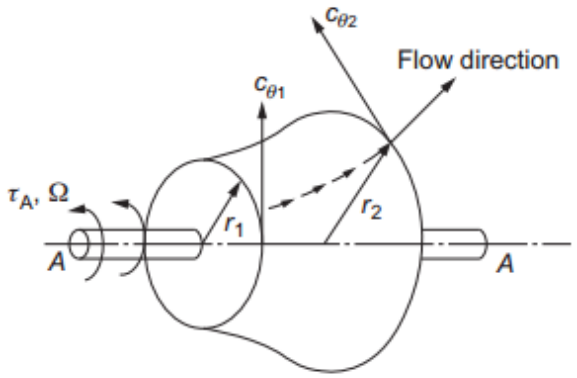

Figure 15: Control volume in a generalized turbomachine [8]

of velocities and flow angles.

7.4 Fluid deviation

In real life situation, the flow leaving the impeller blades does not follow the angle of the blade at the trailing edge. The distance between impeller blades increases as the radius pf impeller increases. This create a diffusor like effect in the blade passages where the flow diffuses and diverges as it gets further away from the leading edge. The flow is less guided by the blades when they are further apart.

Since the surface area of the impeller passage increases along the passage, effective boundary layers increase which causes increased blockage. This increases the flow deviation further.

The deviation is more prominent in impellers with radial flow and little to no deviation in axial flow impellers.

7.5 Rotation free inlet

In a 3D motion, the relationship between absolute flow velocity c and its components of a turbomachine can be written as:

$$c^2 = c_r^2 + c_\theta^2 + c_x^2$$

The same relationship also applies to the relative velocities:

$$w^2 = w_r^2 + w_\theta^2 + w_x^2$$

From the equation of relative velocities, the relative flow velocity w can be written as:

$$w^2 = w_r^2 + (c_\theta - U_\theta)^2 + c_x^2$$

or

$$w^2 = c_r^2 + (c_\theta - U_\theta)^2 + c_x^2$$

since

$$w_r = c_r$$

w_2, c_2, and U_2 are velocities at the trailing edge of the blade with radius x_2 while w_1, c_1, and U_1 are velocities at the trailing edge of the blade with radius x_1.

For a rotation free inlet, flow enters axially into the impeller so the tangential component of the absolute inlet flow velocity $c_{\theta 1} = 0$.

7.5.1 Rotation free inlet in radial impeller

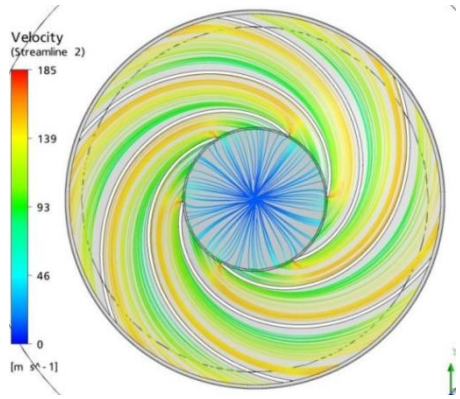

Figure 17: Rotation free inlet in radial impeller with purely radial vanes

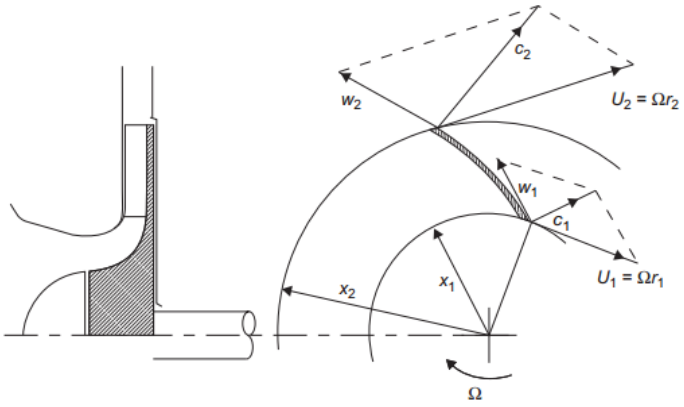

Figure 16: Velocity triangles at impeller with purely radial vanes [8]

Based on Figure 17, the absolute inlet flow velocity c_1 has a whirl component or angular momentum. Figure 16 shows a radial impeller with rotation free inlet.

7.5.2 Rotation free inlet for axial impeller

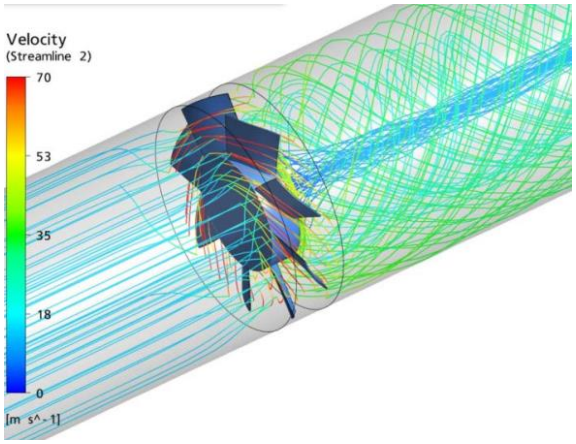

Figure 19: Rotation free inlet in axial flow impeller (propeller) [9]

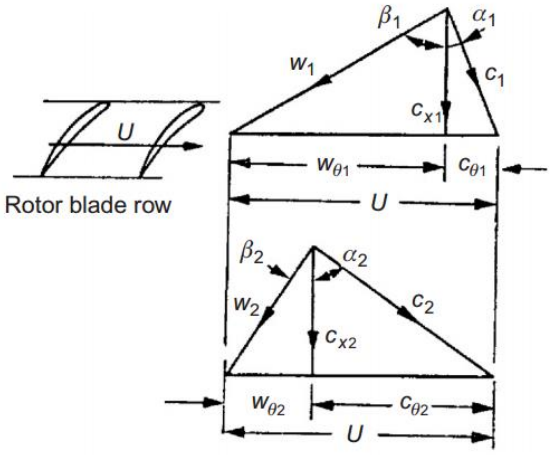

Figure 18: Velocity triangles at an axial flow impeller (propeller) [8]

Figure 19 shows velocity triangles with prerotation. For a rotation free inlet at an axial flow impeller, the absolute inlet flow velocity is also the same, which means $c_{\theta 1} = 0$. This can be seen in figure 18.

7.6 Velocity triangle

Below are the velocity triangles for the leading edge or at inlet (point 1) and trailing edge or outlet (point 2) of the radial, axial, and mixed flow impellers. The velocity triangles at 1 for all impellers are assumed to have rotation free inlet.

7.6.1 Velocity triangle in radial flow impeller

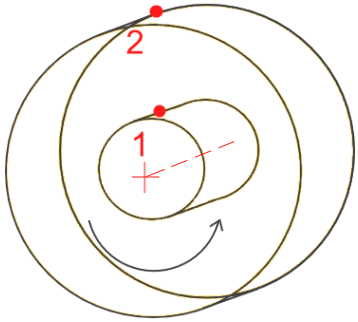

Figure 22: Inlet and outlet point in radial flow impeller with backwards curved vanes

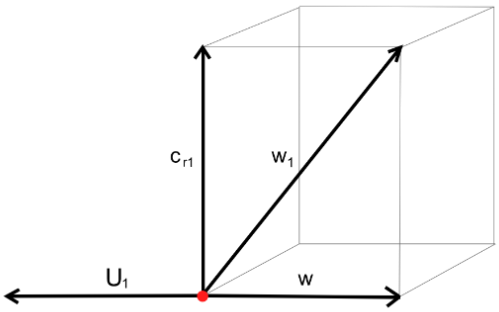

Figure 21: Velocities at radial inlet

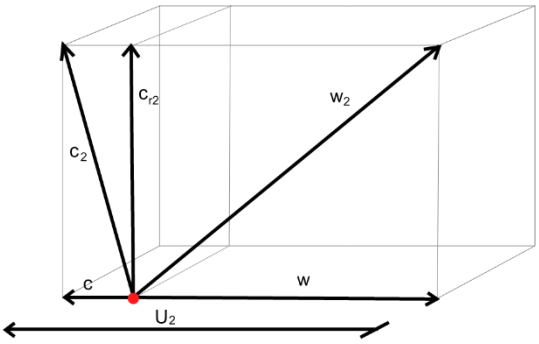

Figure 20: Velocities at radial outlet

The absolute flow velocity and the relative flow velocity do not have components in the axial direction. Thus:

$$c_{x1} = c_{x2} = c_x = w_{x1} = w_{x2} = w_x = 0$$

For a pump with radial impeller with rotation free inlet, the flow rate is the same at inlet and outlet. Therefore, velocities in radial direction should be the same. Since there are no velocity components in the axial direction, the meridian velocity can be defined as:

$$c_{r1} = c_{r2} = c_r = w_{r1} = w_{r2} = w_r = c_m = w_m$$

Also, $U_2 > U_1$ because of the bigger radius at point 2.

7.6.2 Velocity triangle in axial flow impeller

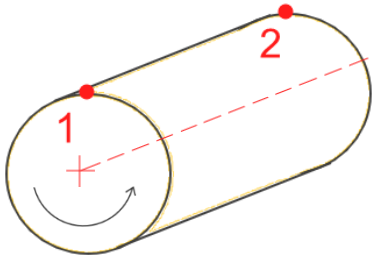

Figure 25: Inlet and outlet point in an axial flow Impeller

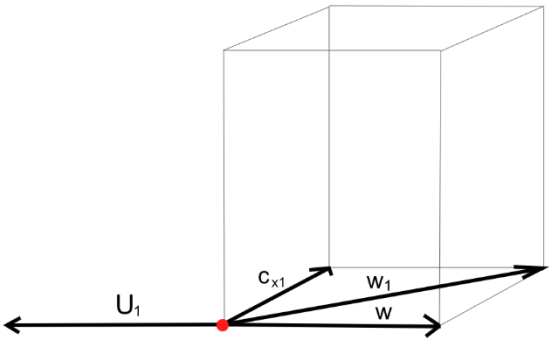

Figure 24: Velocities at axial inlet

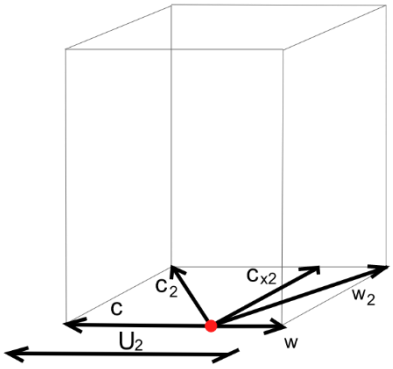

Figure 23: Velocities at axial outlet

It is clear that purely axial flow impellers do not have velocity components in the radial direction. Thus:

$$c_{r1} = c_{r2} = c_r = w_{r1} = w_{r2} = w_r = 0$$

Velocities in axial direction should be the same for an axial impeller with rotation free inlet in an incompressible medium since the flow rate is the same for both inlet and outlet. Since there are no velocity components in the radial direction, the meridian velocity of a purely axial flow impeller is:

$$c_{x1} = c_{x2} = c_x = w_{x1} = w_{x2} = w_x = c_m = w_m$$

Since the radius of impeller tip does not change along the flow path, therefore $U_1 = U_2$.

7.6.3 Velocity triangle in mixed flow impeller

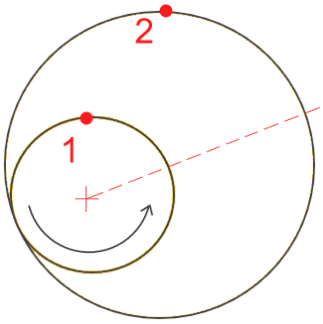

Figure 28: Inlet and outlet point in mixed flow impeller with backward curved vanes

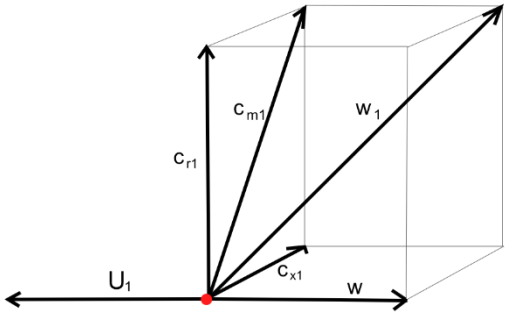

Figure 26: Velocity triangle at mixed flow inlet

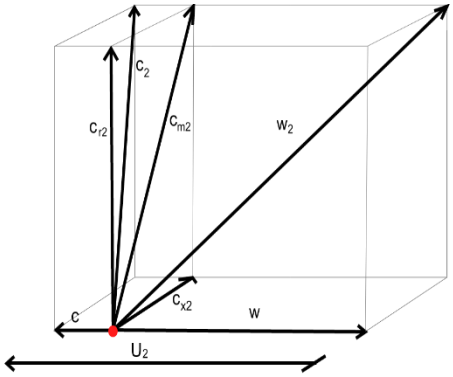

Figure 27: Velocity triangle at mixed flow outlet

Fluid flow in a mixed flow impeller can be fairly complicated to explain as it can only be represented in three dimensions. Mixed flow impellers have velocity components in all direction othr than the afore mentioned no prerotation.

Assuming the impeller is in an incompressible medium, the flow rate will remain the same at point 1 and point 2. Although the radial and axial components of the absolute flow velocity between these two points differ, the vector sum of the radial and axial components between these two points remain the same. It only differs in direction and not the magnitude. These are represented by the meridian velocities:

$$c_{m1} = c_{m2} = w_{m1} = w_{m2} = c_m = w_m$$

Since the radius of impeller tip increases along the flow path, therefore $U_2 > U_1$.

Note that all the velocity components for absolute velocity and relative velocity are represented in the same direction for radial, axial and mixed flow impellers. The direction of the absolute velocity c and radial velocity w at inlet and outlet differs from different impeller flow types because of the different magnitude of the velocity components.

7.7 Slip factor and established models

7.7.1 The slip effect

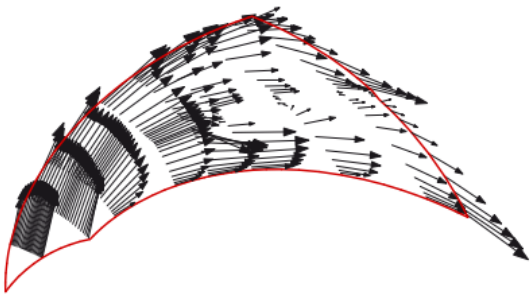

Figure 30: Relative velocity inside vane canal of a radial fan (from CFD simulation) [2]

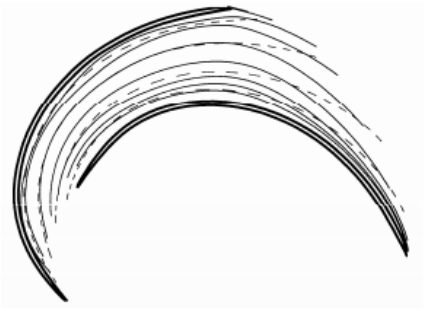

Figure 29: Relative flow path in a radial impeller. Broken lines represent ideal flow path

In an ideal flow, it is assumed that the flow is perfectly guided by the vanes and the flow leaving the vanes have the same angle as the vane tip. the flow is also assumed to be frictionless and the vanes are infinitesimally thin and infinite in number. Other assumptions are the pressure field in the impeller canal has rotation symmetry meaning that no pressure difference exist between the pressure side and the suction side of vanes and rotation symmetry of the velocity field. Based on Figure 30, it is noticeable that as the flow progress, the vane distance increases and the flow has less guidance from the vanes.

In a real flow, the flow is influenced by friction, the number of vanes are finite and the flow does not the vanes exactly. The flow leaves the impeller with the absolute velocity having less tangential component, consequently the relative velocity has a more tangential

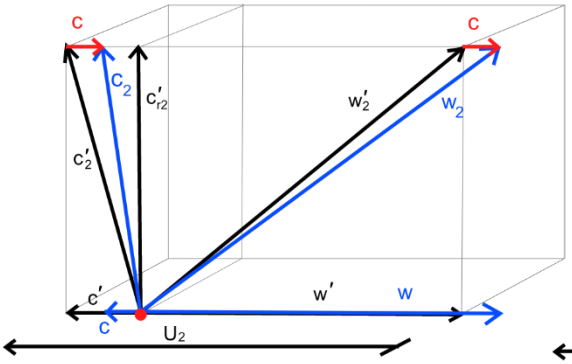

Figure 32: Slip velocity in radial flow impeller

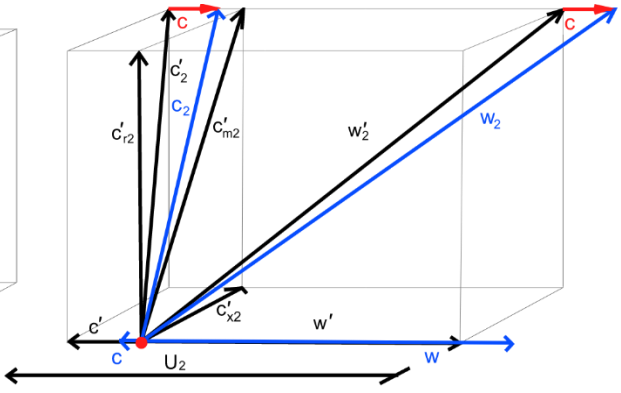

Figure 31: Slip velocity in mixed flow impeller

component. The flow is said to slip.

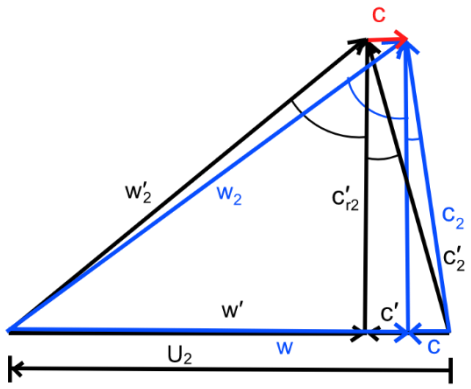

Figure 33: Velocity triangle with slip in radial flow impeller

Figure 32 and Figure 31 describes the phenomena in vector form. Since slip effects the tangential component of the absolute velocity, axial flow impeller is not affected.

This phenomenon can be easier described with a velocity tringle at the trailing edge of a radial flow impeller. The convention in describing slip is that values with a prime symbol (′) are for ideal values without slip while the values without the prime symbol are real values with slip. It is important to not have the values mixed up as earlier chapters of this bachelor thesis explains ideal vectors as per other literatures without the prime symbol.

7.7.2 Flow angle and different vane angle representations

The relationship of the average relative flow angle β_2 or vane angle β_2' to the relative flow velocity components can be obtained using Pythagoras theorem:

$$\beta_2 = \tan^{-1}\left(\frac{w_{\theta 2}}{w_{r2}}\right)$$

$$\beta_2' = \tan^{-1}\left(\frac{w_{\theta 2}'}{c_{m2}}\right)$$

Some literatures describe vane angle as the angle between the w_2' and $w_{\theta 2}'$:

$$\beta_{2b} = \cos^{-1}\left(\frac{w_2'}{w_{\theta 2}'}\right)$$

or

$$\beta_{2b} = \tan^{-1}\left(\frac{c_{m2}}{w_{\theta 2}'}\right)$$

Note that for this definition of blade angle, there is no prime symbol being used.

7.7.3 General definition of slip velocity and slip coefficient

Slip velocity $c_{\theta s}$ is defined as:

$$c_{\theta s} = c'_{\theta 2} - c_{\theta 2}$$

where $c_{\theta 2}$ is the real tangential component of absolute velocity (with slip) and is related to the average relative flow angle β_2 and the hypothetical tangential velocity component of absolute velocity $c'_{\theta 2}$ is related to the exit vane angle β'_2. Zero vane angle means that the vane shape is untwisted and fully radial.

While the slip coefficient or slip factor σ can be defined as:

$$\sigma = \frac{U_2 - c_{\theta s}}{U_2} = 1 - \frac{c_{\theta s}}{U_2}$$

where $\gamma < 1$. Having higher value of slip factor σ means that the flow has lower deviation from the vane.

7.7.4 The relative eddy concept

A simple explanation for slip effect can be made by explaining relative eddy. This is also the basis for early slip theories. Relative eddy is when a fluid has an angular velocity of $-\Omega$ relative to the impeller which has an angular velocity of Ω. This can happen when the absolute flow enters an impeller without spin then leaving the impeller also without spin if

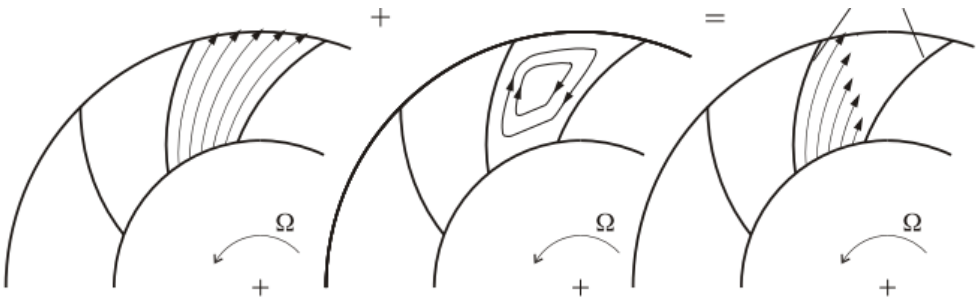

Figure 34: Superposition of through flow and relative eddy [2]

irrotational and frictionless fluid flow passing through an impeller is possible.

Superimposing a through-flow on a relative eddy, results in a relative flow at the outlet of the impeller which will then have the slip effect. The slip effect simply means that the

average relative flow coming from the impeller passages is in opposite direction to the blade motion and at an angle to the vanes.

7.7.5 Slip factor correlations

7.7.5.1 Slip factor estimation model by Wiesner

One of the established slip factor models widely used in the industry is by Wiesner (1967). Wiesner based his calculation on 2D vanes curved as logarithmic spirals. Logarithmic spiral

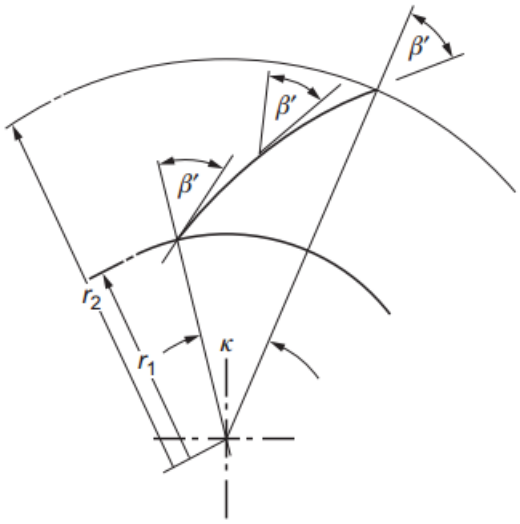

Figure 36: Equiangular or logarithmic spiral vane [8]

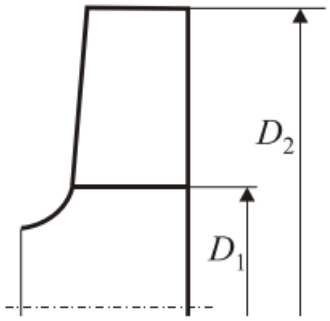

Figure 35: Radii in defining the radius ratio in a radial impeller [2]

vane means that the vane angle β' is constant throughout the impeller radius.

Firstly, a limiting mean radius ratio for the impeller ε_{lim} (correction factor) must be defined:

$$\varepsilon_{lim} = \frac{1}{ln^{-1}\left(8.16 \sin\frac{\beta_{2b}}{Z}\right)}$$

with Z = Number of blades.

Wiesners classical empirical model for determining the slip factor of centripetal impellers are:-

For $\frac{r_1}{r_2} \leq \varepsilon_{lim}$ (without correction factor):

$$\sigma_{Wiesner} = 1 - \frac{\sqrt{\sin\beta_{2b}}}{Z^{0.7}}$$

For $\frac{r_1}{r_2} > \varepsilon_{lim}$ (with correction factor):

$$\sigma_{Wiesner} = \left(1 - \frac{\sqrt{\sin\beta_{2b}}}{Z^{0.7}}\right) \times \left[1 - \left(\frac{\frac{r_1}{r_2} - \varepsilon_{lim}}{1 - \varepsilon_{lim}}\right)^3\right]$$

7.7.5.2 Slip coefficient estimation model by Aungier

Aungiers model is a modified version of Wiesners original empirical equation. For Aungiers model, the limiting mean radius ratio ε_{lim} (correction factor) is:

$$\varepsilon_{lim} = \frac{\sigma - \sin(19° + 0.2\beta_{2b})}{1 - \sin(19° + 0.2\beta_{2b})}$$

with

$$\sigma = 1 - \frac{\sqrt{\sin\beta_{2b}}}{Z^{0.7}}$$

Aungiers model for determining the slip factor of centripetal impellers are:-

For $\frac{r_1}{r_2} \leq \varepsilon_{lim}$ (without correction factor):

$$\sigma_{Aungier} = \sigma = 1 - \frac{\sqrt{\sin\beta_{2b}}}{Z^{0.7}}$$

For $\frac{r_1}{r_2} > \varepsilon_{lim}$ (with correction factor):

$$\sigma_{Aungier} = \sigma\left(1 - \left(\frac{\varepsilon - \varepsilon_{Lim}}{\varepsilon - \varepsilon_{Lim}}\right)^{\sqrt{\beta_{2b}/10}}\right)$$

7.7.5.3 Slip coefficient estimation model by Gülich

Gülich also took Wiesners original formula and modified it but with two additional correction factors, f_1 and k_w. Correction factor f_1 depends on the through flow of the impeller, while k_w depends on the limiting mean radius ratio ε_{lim}.

Just like the other two models, the limiting mean radius ratio ε_{lim} must first be calculated:

$$\varepsilon_{lim} = exp\left(-\frac{8.16\sin\beta_{2b}}{Z}\right)$$

Next, the average inlet diameter d_{1m} must be calculated before the second correction factor k_w can be obtained:

$$d_{1m} = \sqrt{0.5 \cdot \left({d_{1,Shroud}}^2 + {d_{1,Hub}}^2\right)}$$

For $\frac{d_{1m}}{d_2} \leq \varepsilon_{lim}$:

$$k_w = 1$$

For $\frac{d_{1m}}{d_2} > \varepsilon_{lim}$:

$$k_w = 1 - \left(\frac{\frac{d_{1m}}{d_2} - \varepsilon_{lim}}{1 - \varepsilon_{lim}} \right)^3$$

For radial impellers:

$$f_1 = 0.98$$

For mixed-flow impellers:

$$f_1 = 1.02 + 1.2 \cdot 10^{-3}(n_q - 50)$$

with n_q = specific speed of impeller in [1/min]

$$n_q = n \cdot \frac{Q^{1/2}}{H^{3/4}}$$

with Q = head in [m]

H =flow rate in [m^3/h]

For $\frac{d_{1m}}{d_2} \leq \varepsilon_{lim}$ (without correction factors):

$$\sigma_{Gülich} = \sigma = 1 - \frac{\sqrt{\sin \beta_{2b}}}{Z^{0.7}}$$

For $\frac{d_{1m}}{d_2} > \varepsilon_{lim}$ (with correction factors):

$$\sigma_{Gülich} = f_1 \cdot \left(1 - \frac{\sqrt{\sin \beta_{2b}}}{Z^{0.7}} \right) \cdot k_w$$

7.7.5.4 Slip factor estimation model by Pfleiderer

The empirical slip correlation for pumps brought by Pfleiderer considers the impeller geometry, blade loading, as well as downstream collecting system (volute or diffuser).

The reduced performance factor μ is generally defined as:

$$\mu = \frac{Y_{th}}{Y_{th\infty}} = \frac{c_{\Theta 2}}{c'_{\Theta 2}}$$

with

Y_{th} = Specific work by vane in real flow

$Y_{th\infty}$ = Specific work by vane in ideal flow

Pfleiderer expressed reduced performance factor μ based on his research as:

$$\mu = \frac{1}{1 + 2\frac{\psi'}{Z}\frac{1}{1 - \left(\frac{d_1}{d_2}\right)^2}}$$

with $d_1/d_2 = r_1/r_2$

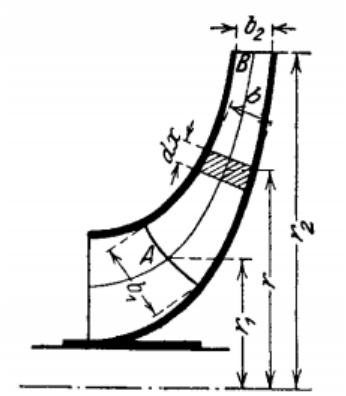

Figure 37: Meridian cross section of a radial impeller in a pump [10]

and experience number ψ' :

$$\psi' = a\left(1 + \frac{\beta_{2b}}{60°}\right)$$

with the constant a:

for radial impeller	with guided vanes	$a = 0.6$
	with volute	$a = 0.65$ ... 0.84
	with plain diffusor	$a = 0.85$ ... 1.0
for mixed flow/ axial impeller	-	$a = 1.0$ ... 1.2

Rearranging the general formula for reduced performance factor gives:

$$c_{\Theta 2} = \mu \cdot c'_{\Theta 2}$$

and inserting it into the slip velocity formula will give:

$$c_{\theta s} = c'_{\theta 2} - \mu \cdot c'_{\theta 2} = c'_{\theta 2} \cdot (1 - \mu)$$

To get the ideal absolute tangential velocity of the flow at outlet, the ideal relative tangential velocity must first be obtained:

$$\tan \beta_{2b} = \frac{c_m}{w'_{\theta 2}}$$

Rearranging this formula gives:

$$w'_{\theta 2} = \frac{c_m}{\tan \beta_{2b}}$$

and after subtracting it from peripheral velocity U_2 will give:

$$c'_{\theta 2} = U_2 - \frac{c_m}{\tan \beta_{2b}}$$

From this, the slip factor estimation based on Pfleiderer can be derived:

$$\sigma_{Pfleiderer} = 1 - \frac{c'_{\theta 2} \cdot (1 - \mu)}{U_2}$$

8 Mesh refinement study

8.1 Mesh refinement overview

Computational fluid dynamics (CFD) is a tool used by engineers to predict the real-world scenarios using computational models. The computer-aided-design (CAD) model is modified to give a negative form, representing the volumes in and surrounding the model. The volume will then be subdivided into smaller domains called cells, over which a set of equations related to the flow characteristics will be calculated or 'solved'. The equations related to the flow characteristics are approximation of the governing equations with polynomials defined over each cell. Therefore, as the number of cells increase, the closer is the solution to a real-world value. An infinite number of cells would be theoretically give the best solution but also have the negative effect of increasing the computational load and simulation time. Therefore, a compromise must be made to have a 'good enough' mesh that

gives great approximate solution and short simulation time. The method in obtaining the most suitable mesh for a simulation is called the mesh refinement study.

Mesh refinement study is an important step before proceeding to start multiple simulations as it also builds the users confidence in the physical simulation model used, and the result of the simulation. Knowledge of the constraints and boundary conditions as well as the physical properties of the fluid region is important in doing mesh refinement study as it will affect the

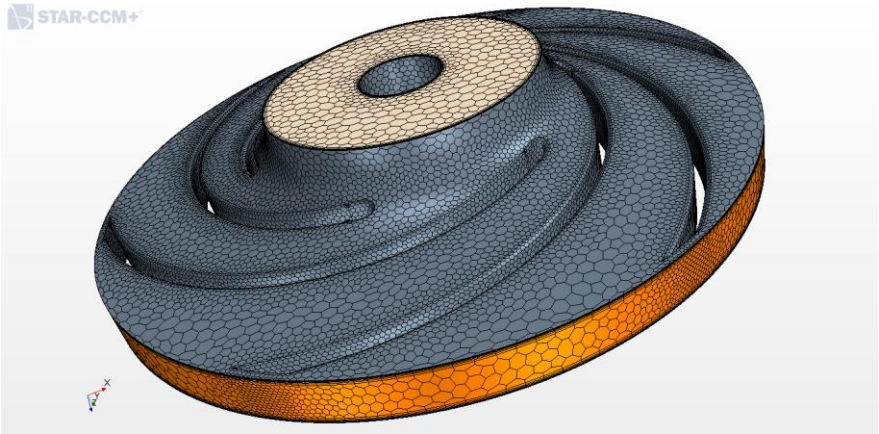

Figure 38: Preliminary mesh

result of interest of the simulation greatly.

The first step in mesh refinement study is to have a preliminary mesh. The preliminary mesh should be the most course among other meshes. The idea is to simulate a case with the least computational resource and successively using finer and finer meshes while comparing the results of interest for difference and fluctuations. Generally, the difference of 1% in values of interest between refinements is considered negligible and considers the mesh prior to the refinement to be acceptable.

8.2 Single case simulation setup for mesh refinement study

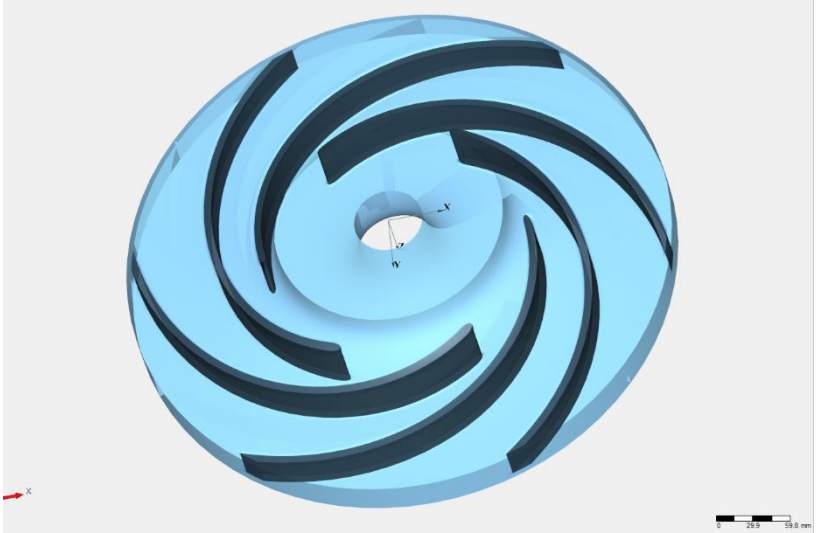

Figure 39: Impeller blade in CFturbo

The following setup was made in simulation software Star-CCM+ to the impeller geometry file 'RP nq20 volute (generic)' taken from turbomachinery geometry generation software CFturbo's radial pump example folder:

Original file name : RP nq20 volute Generic)_Co1.stp

Density : 998.2 kg/m^3

Dynamic viscosity : $9.982\times10^{-4}\ Pa\cdot s$

Mass flow rate : 16.637 kg/s

Number of revolutions : 2900 rpm

Turbulence model used: K-Epsilon with realizable K-Epsilon two layer*

to measure the total pressure difference between Inlet and Outlet ΔP_t in [Pa], radial (Meridian) flow velocity at impeller outlet w_m in [m/s], and relative tangential flow velocity at impeller outlet $w_{\theta 2}$ in [m/s].

Detailed setup method from geometry generation to simulation can be found in [2].

**Naturally, K-Omega Turbulence with SST (Menter) K-Omega is preferred over the chosen turbulence model because of its many benefits over K-Epsilon, but during simulation, it is found that K-Omega turbulence model on Star-CCM+ was having some stability problems for the chosen turbomachine, hence K-Epsilon turbulence model was chosen instead.*

8.3 Formulas for calculating difference and fluctuation of values of interest between mesh refinements

The difference dif_i is calculated by:

$$dif_i = |V_i - V_{i-1}|$$

for $i = 2\,, 3,\ 4, \ldots n$

$n = number\ of\ refinements$

$V_i = Value\ of\ interest\ (w_m;\ w_{\Theta 2};\ \Delta P_t)$

and $i = 1$ is the preliminary mesh.

While the formula for percentage difference $dif_{\%,i}$ is:

$$dif_{\%,i} = \frac{dif_i}{V_{i-1}} \times 100\%$$

8.4 Mesh refinement techniques

8.4.1 Reduction in base size.

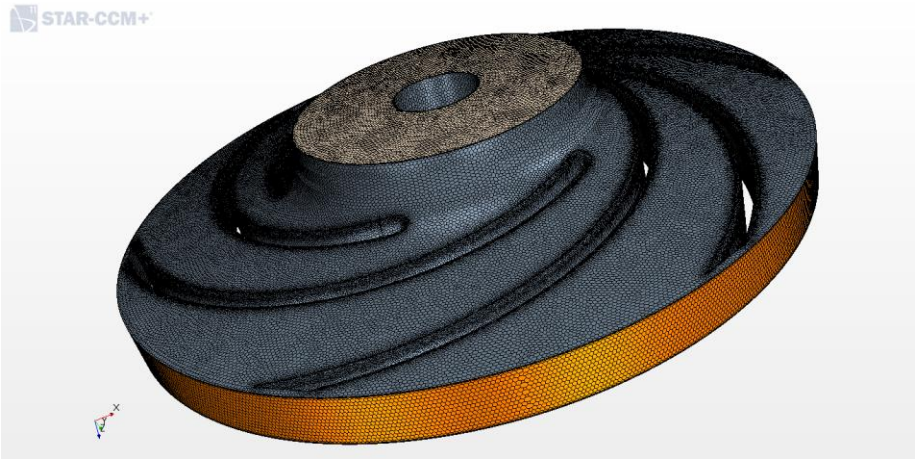

Figure 40: Refined mesh

This method globally minimizes the cell size of the model. This approach is the most common as it is simple. This method addresses the mesh refinement needed for the regions

with more errors. This method has a drawback however as regions that doesn't need more exact solutions are also refined.

For the base size comparison, variations of base cell base sizes from 5mm to 1mm were made and the results were then analyzed. Other variables such as number of prism layers, prism layer stretching and number of iterations were kept constant.

Table 1: Base size variations with results

Base size	# Prism layer	Iterations	rad vel [m/s]	rel tan vel [m/s]	total pressure dif [Pa]	last Iteration time [s]	Sim. time [min]	# Cells
5mm	2	400	2.474772	-12.37079	707553.9	1.177	7.85	125133
4mm	2	400	2.438022	-12.35517	712696.5	1.604	10.69	170961
3mm	2	400	2.405151	-11.88792	724014.5	2.634	17.56	273277
2mm	2	400	2.879224	-16.30564	659665.5	5.708	38.05	510347
1.9mm	2	400	2.821906	-15.45769	673586.7	5.601	37.34	555135
1.8mm	2	400	2.372429	-11.62949	733888.2	5.710	38.07	612038
1.7mm	2	400	2.939302	-16.75854	652992.1	6.230	41.53	683954
1.6mm	2	400	2.985648	-16.47225	657316.1	9.320	62.13	791759
1.5mm	2	400	2.944675	-16.15339	664065.1	10.441	69.61	895261
1.4mm	2	400	3.024364	-17.06648	648824.7	11.433	76.22	1009467
1.3mm	2	400	3.007177	-17.19867	647329.2	13.719	91.46	1155919
1.2mm	2	400	3.208284	-18.31334	627966.1	14.683	97.89	1342302
1.1mm	2	400	3.332112	-17.99044	639006.9	16.977	113.18	1607523
1mm	2	400	3.418693	-17.93879	641594.3	25.147	167.65	2001351

Table 2: Base size comparison

Base size comparison					
Difference			Percentage Difference		
rad vel [m/s]	rel tan vel [m/s]	total pressure dif [Pa]	rad vel [m/s]	rel tan vel [m/s]	total pressure dif [Pa]
-	-	-	-	-	-
0.036750	0.015620	5142.6	1.5%	0.1%	1%
0.032871	0.467250	11318.0	1.3%	3.8%	2%
0.474073	4.417720	64349.0	19.7%	37.2%	9%
0.057318	0.847950	13921.2	2.0%	5.2%	2%
0.449477	3.828200	60301.5	15.9%	24.8%	9%
0.566873	5.129050	80896.1	23.9%	44.1%	11%
0.046346	0.286290	4324.0	1.6%	1.7%	1%
0.040973	0.318860	6749.0	1.4%	1.9%	1%
0.079689	0.913090	15240.4	2.7%	5.7%	2%
0.017187	0.132190	1495.5	0.6%	0.8%	0%
0.201107	1.114670	19363.1	6.7%	6.5%	3%
0.123828	0.322900	11040.8	3.9%	1.8%	2%
0.086581	0.051650	2587.4	2.6%	0.3%	0%

Refinement of base size from 1.3mm to 1.2mm shows negligible percentage difference of less than 1% therefore 1.3mm base size is accepted.

8.4.2 Increase in number of prism layers and reduction in prism layer stretching

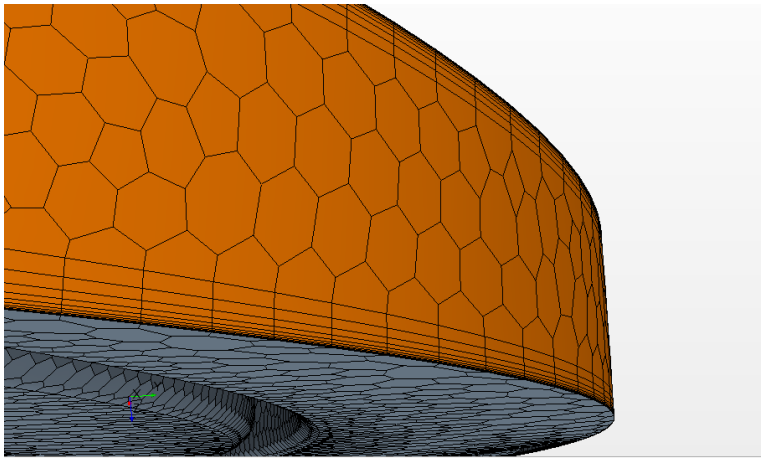

Figure 41: Prism layer stretching at 50%

The details about boundary layer in a fluid flow can be captured using prism layer mesh. Since prism layer mesh only applies to near wall regions, this method greatly increases the accuracy of the solution and a very cost effective method in giving good convergence while not having to do fine meshing globally.

Prism layer stretching used by in mesh refinement study by default is 1.5. This means that the thickness of each cell layer as a ratio to the previous layer is 150%. Prism layer stretching of 1.2 was also tested and observed. This is because theoretically, lower prism layer stretching will give better results as it can capture the velocity profile of the fluid near the wall better.

For both cases, multiple number of prism layers from 2 to 10 layers were tested.

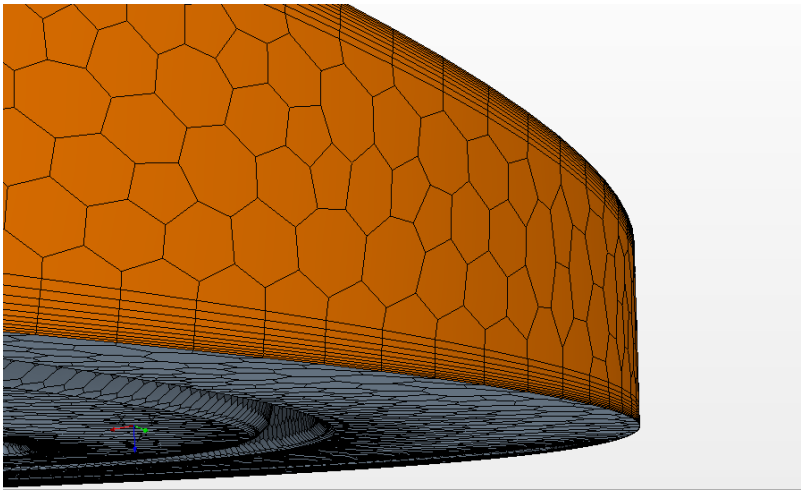

Figure 42: Prism layer stretching at 20%

Table 3: Prism layer variations with results

Base size	# Prism layer	Iterations	rad vel [m/s]	rel tan vel [m/s]	total pressure dif [Pa]	last Iteration time [s]	Sim. time [min]	# Cells
5mm	2	400	2.474772	-12.37079	707553.9	1.177	7.85	125133
5mm	3	400	2.507673	-12.74978	703867.0	1.452	9.68	159862
5mm	4	400	2.643466	-13.68302	688280.4	1.730	11.53	194476
5mm	5	400	2.621064	-13.83674	685154.7	1.867	12.45	229225
5mm	6	400	2.594651	-13.44258	689792.9	2.158	14.39	263977
5mm	7	400	2.825226	-14.93483	667604.7	2.475	16.50	298774
5mm	8	400	2.679529	-15.32726	659278.2	3.335	22.23	333579
5mm	9	400	2.710656	-14.31084	675904.9	3.231	21.54	368409
5mm	10	400	2.664157	-14.51903	673717.1	3.090	20.60	403111
5mm	(stretching 1,2) 2	400	2.482334	-12.52499	704664.5	1.461	9.74	125117
5mm	(stretching 1,2) 3	400	2.498381	-12.95465	699123.1	1.341	8.94	159701
5mm	(stretching 1,2) 4	400	2.435695	-11.99832	713983.4	2.163	14.42	194332
5mm	(stretching 1,2) 5	400	2.641707	-13.90512	683842.9	2.732	18.21	228801
5mm	(stretching 1,2) 6	400	2.702021	-13.80927	686133.3	2.296	15.31	263413
5mm	(stretching 1,2) 7	400	2.633440	-13.35849	691544.6	2.453	16.35	298091
5mm	(stretching 1,2) 8	400	2.569925	-13.22406	694088.8	4.113	27.42	332639
5mm	(stretching 1,2) 9	400	2.619857	-13.69175	686079.4	4.209	28.06	367308
5mm	(stretching 1,2) 10	400	2.594460	-13.53459	688559.3	3.529	23.53	402041

Table 4: Prism layer comparison

Prism layer comparison					
Difference			Percentage Difference		
rad vel [m/s]	rel tan vel [m/s]	total pressure dif [Pa]	rad vel [m/s]	rel tan vel [m/s]	total pressure dif [Pa]
-	-	-	-	-	-
0.032901	0.378990	3686.9	1.3%	3.1%	0.5%
0.135793	0.933240	15586.6	5.4%	7.3%	2.2%
0.022402	0.153720	3125.7	0.8%	1.1%	0.5%
0.026413	0.394160	4638.2	1.0%	2.8%	0.7%
0.230575	1.492250	22188.2	8.9%	11.1%	3.2%
0.145697	0.392430	8326.5	5.2%	2.6%	1.2%
0.031127	1.016420	16626.7	1.2%	6.6%	2.5%
0.046499	0.208190	2187.8	1.7%	1.5%	0.3%
-	-	-	-	-	-
0.016047	0.429660	5541.4	0.6%	3.4%	0.8%
0.062686	0.956330	14860.3	2.5%	7.4%	2.1%
0.206012	1.906800	30140.5	8.5%	15.9%	4.2%
0.060314	0.095850	2290.4	2.3%	0.7%	0.3%
0.068581	0.450780	5411.3	2.5%	3.3%	0.8%
0.063515	0.134430	2544.2	2.4%	1.0%	0.4%
0.049932	0.467690	8009.4	1.9%	3.5%	1.2%
0.025397	0.157160	2479.9	1.0%	1.1%	0.4%

Although relative tangential velocity has not ‘converged’ very well up until 10 prism layers in both stretching of 1.5 and 1.2, the best convergence setup from the mesh refinement study of 10 prism layers with 20% stretching was accepted. This is because the number of cells have already reached a high number of around 400,000 when base size is by 5mm. For finer base sizes, the cell count can grow exponentially higher and this should be avoided.

8.4.3 Increase in number of iteration

Simulations that are setup properly will have its residual values converge. A good enough a convergence can be decided visually by visualization of the residual plot during the

simulation or can be calculated empirically my comparing results between iterations or number or defined iterations. Higher iterations give more exact solutions.

Keeping the base size as prism layer number constant, multiple iterations were ran from 200 iterations to 1000.

Table 5: Variations in number of iterations with results

Base size	# Prism layer	Iterations	rad vel [m/s]	rel tan vel [m/s]	total pressure dif [Pa]	last Iteration time [s]	Sim. time [min]	# Cells
1mm	2	200	2.820862	-15.75527	661689.2	25.030	83.43	2001351
		300	3.044053	-15.60834	675533.7	23.711	118.56	2001351
		400	3.418693	-17.93879	641594.3	25.147	167.65	2001351
		500	3.224788	-17.96735	634645.9	21.202	176.68	2001351
		600	3.222445	-18.12307	632779.2	19.775	197.75	2001351
		700	3.253417	-18.26531	630764.1	21.031	245.36	2001351
		800	3.237216	-18.20842	631219.3	20.347	271.29	2001351
		900	3.241494	-18.21840	631292.5	20.293	304.39	2001351
		1000	3.242611	-18.22755	631126.2	21.281	354.68	2001351

Table 6: Comparison of number of iterations

Iteration comparison					
Difference			Percentage Difference		
rad vel [m/s]	rel tan vel [m/s]	total pressure dif [Pa]	rad vel [m/s]	rel tan vel [m/s]	total pressure dif [Pa]
-	-	-	-	-	-
0.223191	0.146930	13844.5	7.9%	0.9%	2.1%
0.374640	2.330450	33939.4	12.3%	14.9%	5.0%
0.193905	0.028560	6948.4	5.7%	0.2%	1.1%
0.002343	0.155720	1866.7	0.1%	0.9%	0.3%
0.030972	0.142240	2015.1	1.0%	0.8%	0.3%
0.016201	0.056890	455.2	0.5%	0.3%	0.1%
0.004278	0.009980	73.2	0.1%	0.1%	0.0%
0.001117	0.009150	166.3	0.0%	0.1%	0.0%

According to the results, from 600 iterations, increase in iteration count will have negligible effect on the percentage difference of the three values of interest.

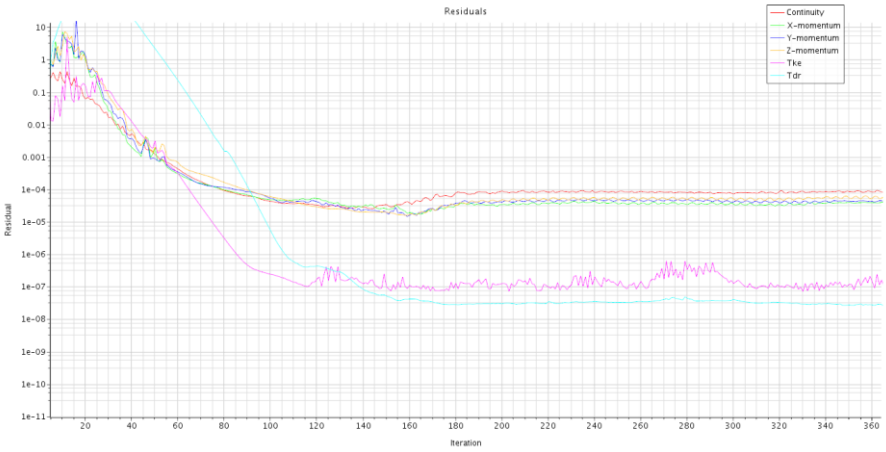

Figure 43: Convergence of residuals

8.4.4 Global adaptive mesh refinement

Local adaptive mesh refinement is an automated method that evaluates the entire region for errors and does adaptive refinement of the mesh at some subset of the entire model space where the errors are significantly larger for higher accuracy of solution. Remeshing of the entire region will still occur but more sensitivity in the error region means that the method is more superior to purely global base size refinement. The disadvantage is that user will not have control over the mesh refinement process.

8.4.5 Summary of mesh refinement study

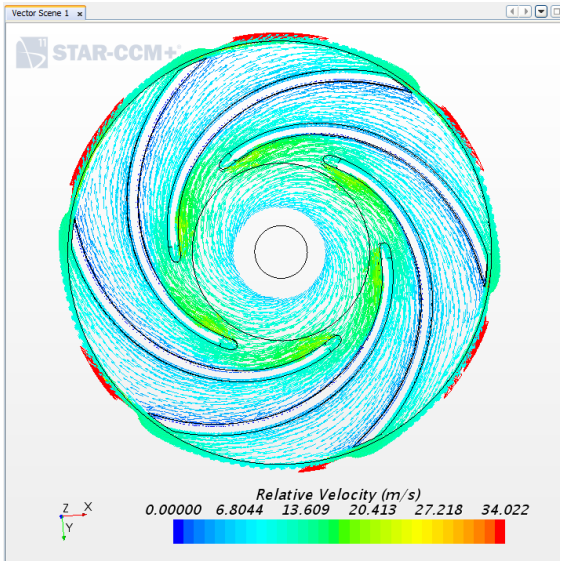

Figure 45: Preliminary mesh simulation

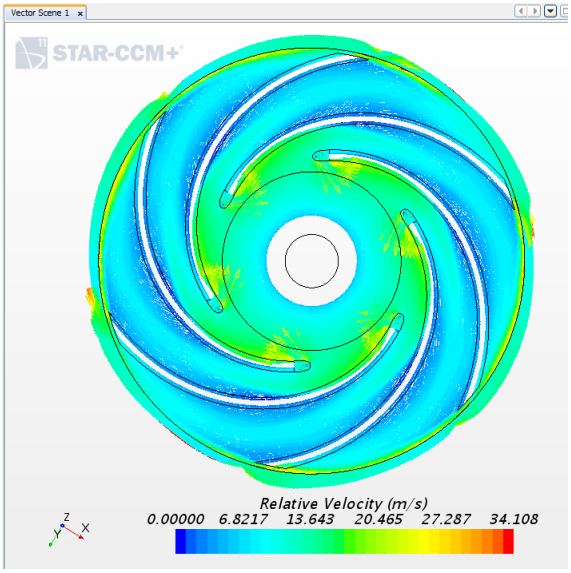

Figure 44: Refined mesh simulation

To summarize, simulations that will be done will have the following mesh settings:

Base size	: 1.3mm
Number of prism layer	: 10
Prism layer stretching	: 1.2
Number of iterations	: 600

Based on experience, number of iterations needed for a ‘good convergence’ will be far less for a finer mesh. Thus, number of iterations might be reduced in actual simulation.

8.5 Periodic boundary condition

For rotating components that have repeated flow distribution pattern or cyclic symmetry for example an impeller, it is sufficient to simulate the periodic section of the component with periodic boundary condition. This allows the flow within the blade passages to be captured without the need to use the full component geometry, therefore minimizing the cell count of the mesh. Applying this boundary condition to the periodic faces of the periodic section will generate a similar mesh structure on periodic faces. This is because the solution values from each periodic faces should be similar.

CFturbo allows users to export the impeller geometry as full geometry as well as a periodic section. This saves time as the user themselves does not have to prepare a periodic section from the full geometry to simulate in CFD. In Star CCM+, the user only needs to define the periodic faces and axis of rotation and the program will automatically calculate the angle the periodicity of the component as well as check the periodic faces for validity.

8.5.1 Comparing full geometry to periodic section of an impeller

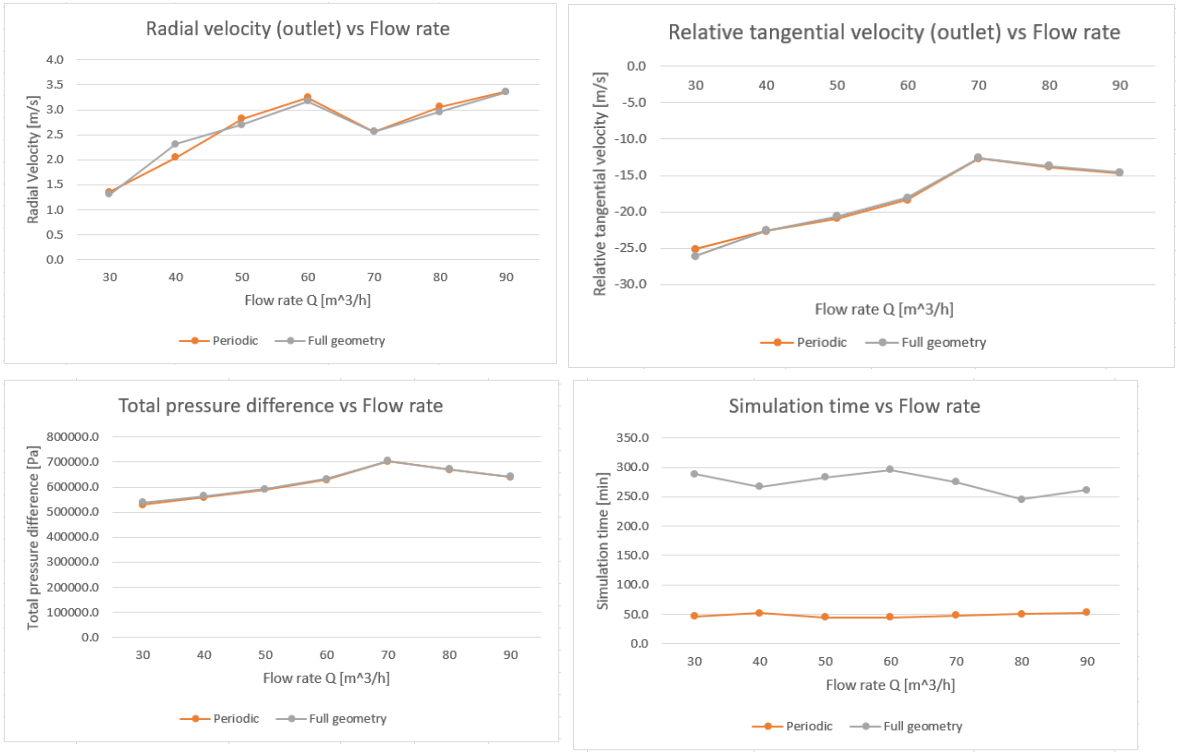

Figure 46: Effects of periodic impeller segment in simulation results

A periodic segment of the impeller geometry 'RP nq20 volute (generic)' was generated and exported from CFturbo. Both the periodic segment and the full geometry were meshed using the same setting in Chapter 0 and then simulated in Star-CCM+. The results of the simulation can be found in Figure 46. Comparing the two geometries, it is seen that the periodic segment gives very similar results in getting the radial (flow) velocity at impeller outlet, relative tangential velocity at impeller outlet and the total pressure difference between the outlet and inlet. The results differ just slightly at lower flow rates.

But when comparing the time taken to simulate the same cases, the full geometry takes significantly more time to get the results with durations taking up to 5 hours. The periodic segment however took roughly 50 minutes to finish simulating. This means that simulating with a periodic segment is almost 5 times faster than with the full geometry.

Hence, periodic boundary will be used for the actual simulations in the next chapters.

9 Slip factor variables & effects

9.1 Methodic

An impeller with the following dimensions and design points was used as a reference:

$$Average\ inlet\ diameter\ d_{1m} = 61mm$$

$$Outlet\ width\ b_2 = 15mm$$

$$Inlet\ vane\ angle\ \beta_1 = 10.7°$$

$$Outlet\ vane\ angle\ \beta_{2b} = 19.9°$$

$$Number\ of\ blades\ Z = 6$$

$$Rate\ of\ rotation\ n = 2900\ rpm$$

$$Wrap\ angle\ \varphi = 129.9°$$

$$Dynamic\ viscosity\ \mu = 9.982 \cdot 10^{-4}\ \frac{Ns}{m^2}$$

$$Flow\ rate\ Q = 60m^3/h$$

To in order to see the individual parameters effects on the slip factor, one parameter will be varied and a simulation would be done for each variation. each parameter change will also be coupled with varying flow rates to visualize the effects the parameter has on the turbomachine throughout the flow rate range. The head curve for each parameter variations will also be available in the attachments as excel file.

9.2 Effects of kinematic viscosity on slip factor

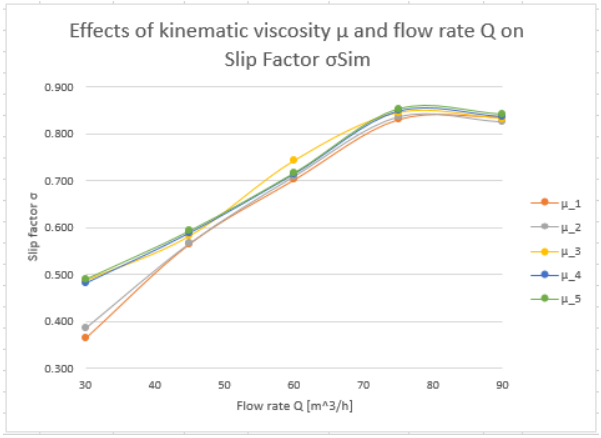

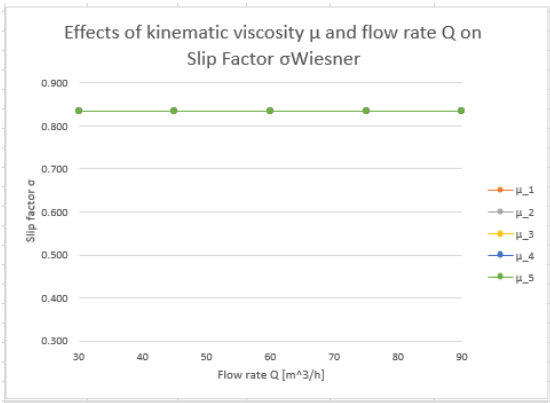

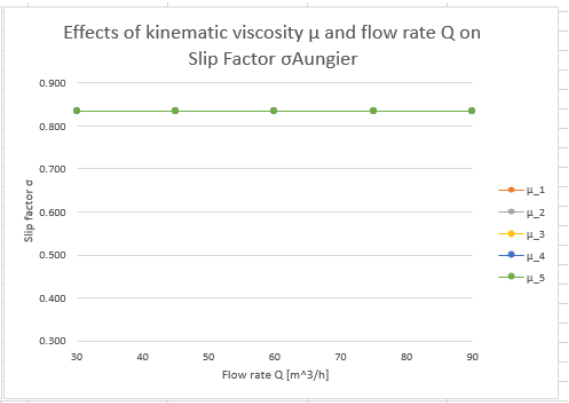

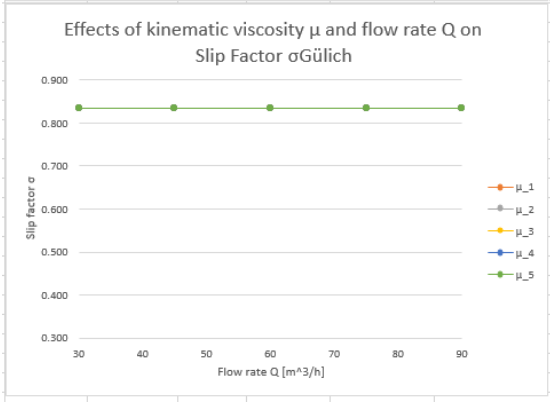

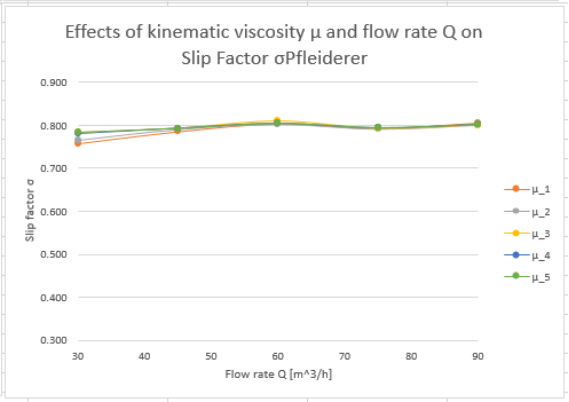

The following are values for different kinematic viscosities tested (in Ns/m^2):

i	1	2	3	4	5
μ_i	$9.982 \cdot 10^{-4}$	0.005	0.010	0.015	0.020

Kinematic viscosity can be seen influencing the slip factor at lower flow rates. The flow of luid with lower viscosities are harder to guide in the impeller canal.

9.3 Effects of wrap angle on slip factor

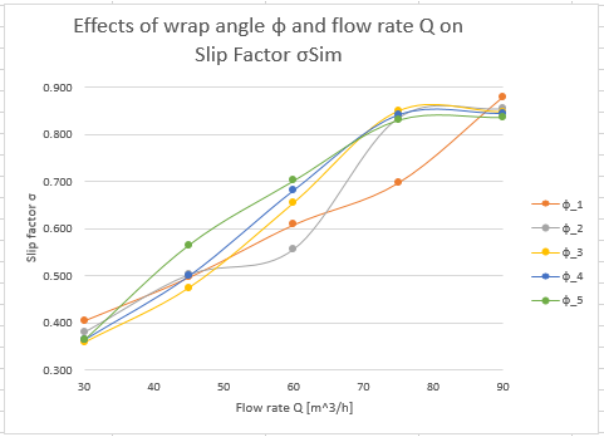

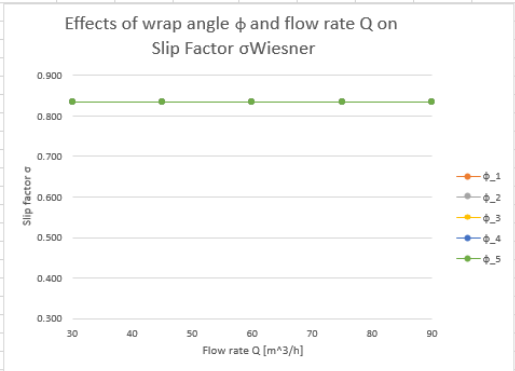

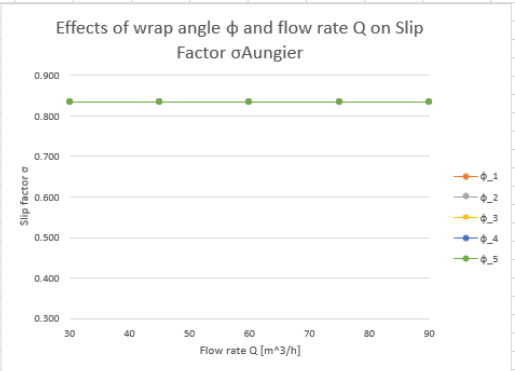

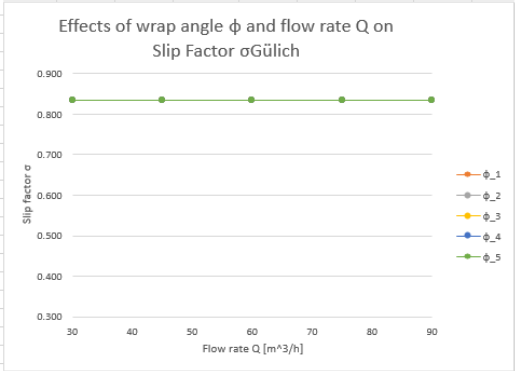

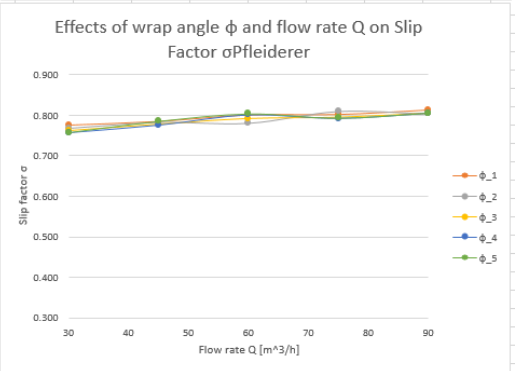

The following are values for different wrap angles simulated:

i	1	2	3	4	5
φ_i	90°	100°	110°	120°	129.9°

For backward curved vanes, the slip factor behaves quadratically with increasing vane angle. As flow rate increases, the minimum point of slip factor will shift towards the lower blade angles. Between the measured slip factor models, Pfleiderers model shows the furthest prediction.

9.4 Effects of rate of rotation

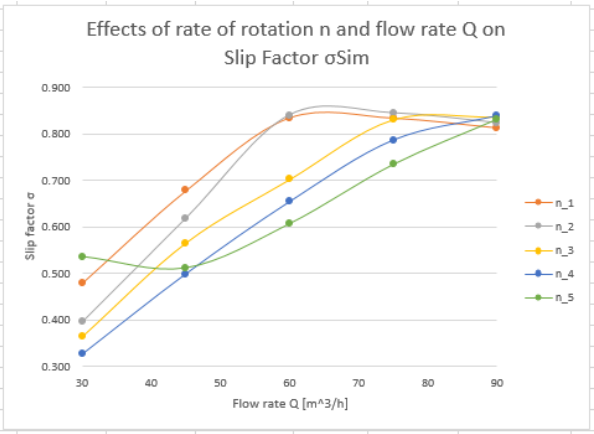

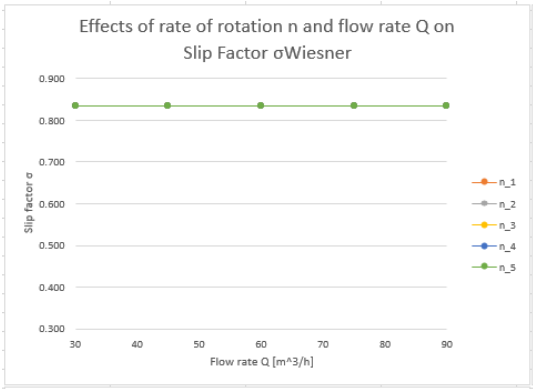

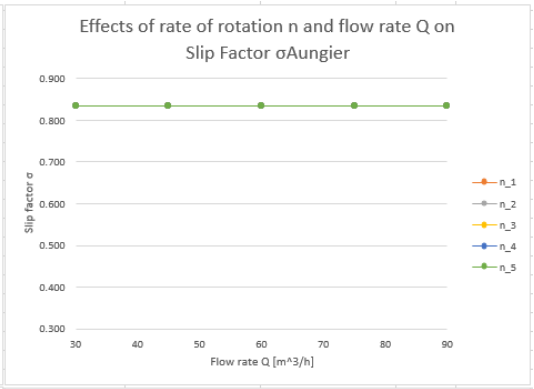

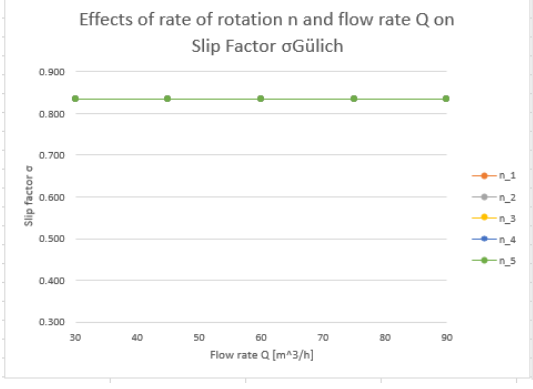

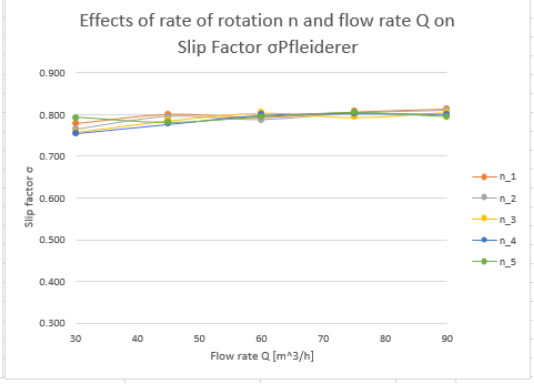

i	1	2	3	4	5
n_i	2340 rpm	2580 rpm	2900 rpm	3180 rpm	3480 rpm

Comparing rate of rotations, it is seen that slip factor decreses with rate of rotation except for a very high rate of rotation which will cause the slip factor to significantly increase. Further test with very high rate of rotations can be made to check wether the increase is exponential. Pfleiderers slip model gives the best prediction in terms variations in rate of rotation and flow rate but as in the shape of the curves only that the curves shift downwards. Wiesners model and the other two variants again made the best prediction at design point.

9.5 Effects of number of vanes on slip factor

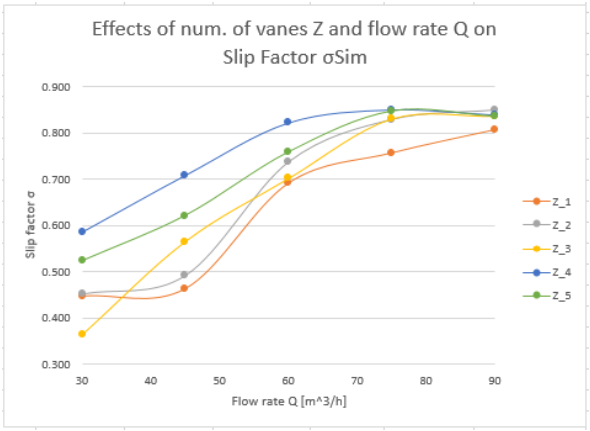

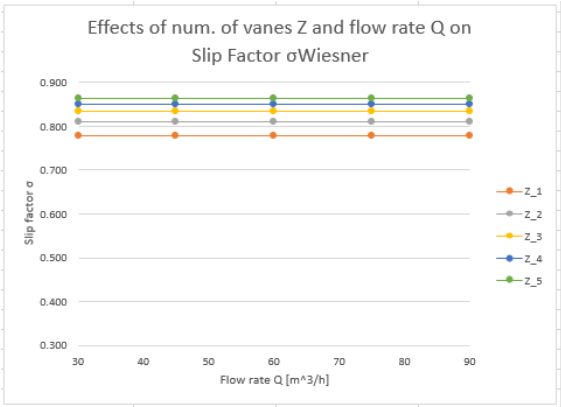

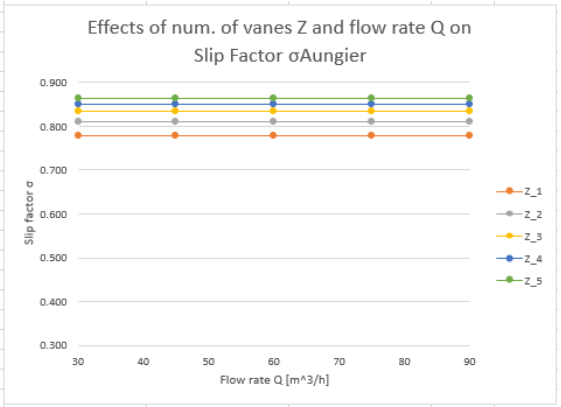

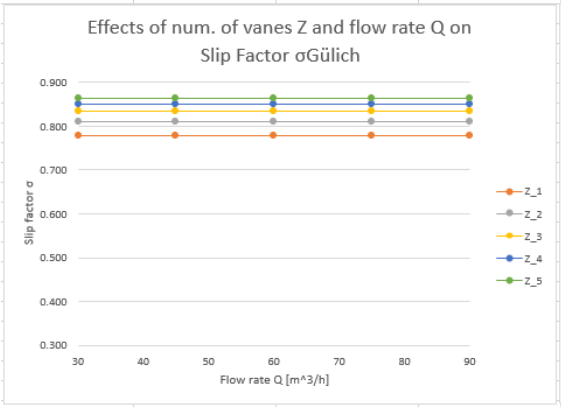

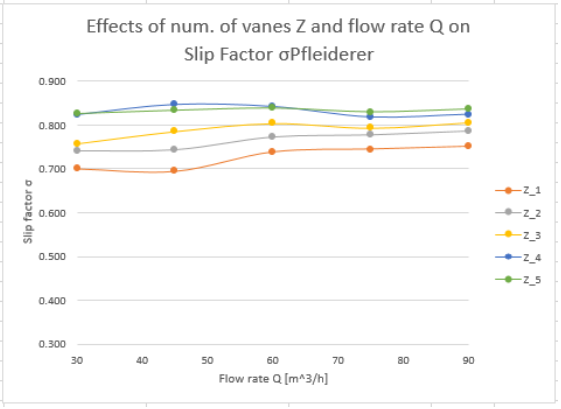

i	1	2	3	4	5
Z_i	4	5	6	7	8

All four models are very similar in describing the effects of number of vanes on slip factor with lowest number of vanes having the least slip factor. The simulation results however show that this is valid up to a certain number of vanes. Too many vanes will decrease the

slip factor as shown by the green curve. All of the models made good prediction of at design point flow rate.

9.6 Effects of outlet vane angle on slip factor

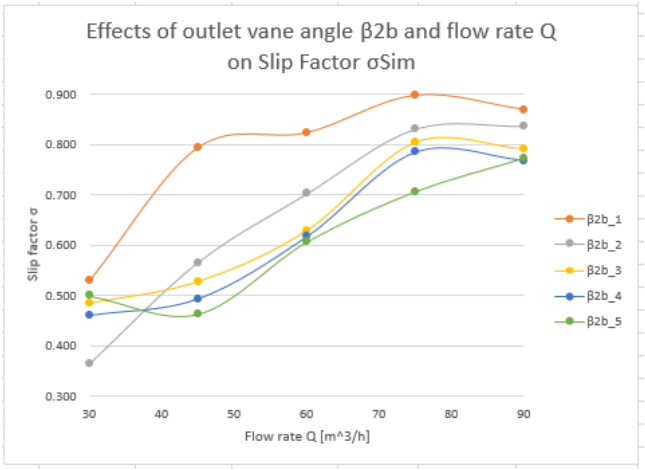

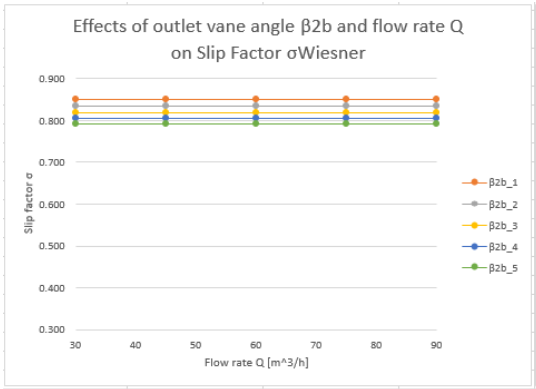

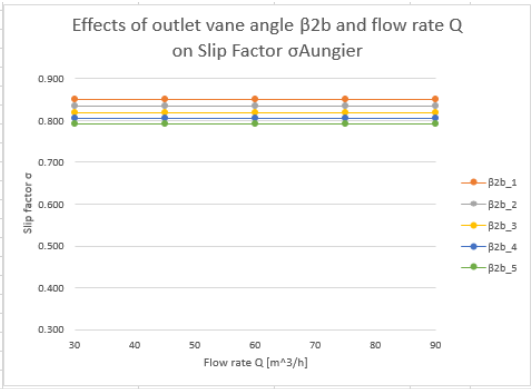

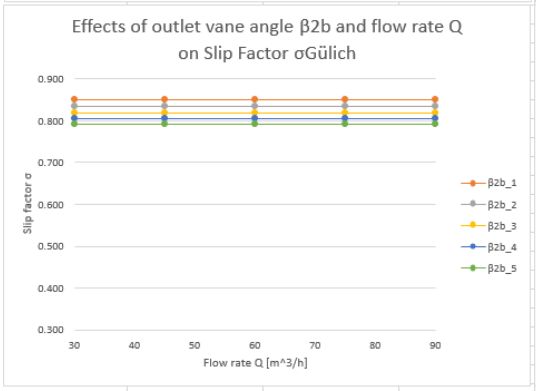

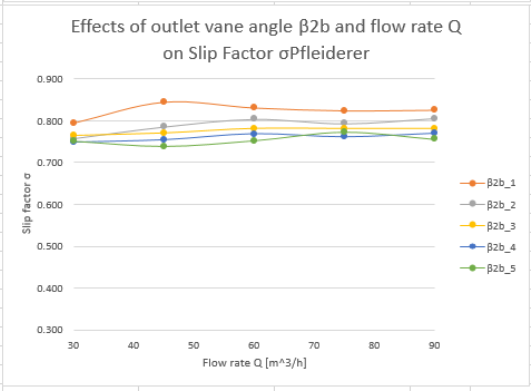

i	1	2	3	4	5
β_{2b_i}	16°	19.9°	24°	28°	32°

Here, all models made the correct prediction that lower outlet vane angle have the highest slip factor but Pfleiderers model goes a bit further as it even provided the signature ‘bump’

in slip factor at the lowest number of blades that the simulation has. Prediction of outlet vane angle effects on slip factor is best at higher flow rates.

9.7 Effects of inlet vane angle on slip factor

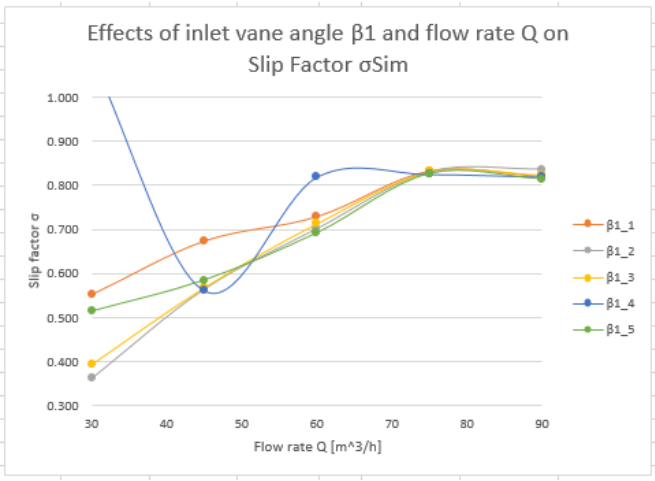

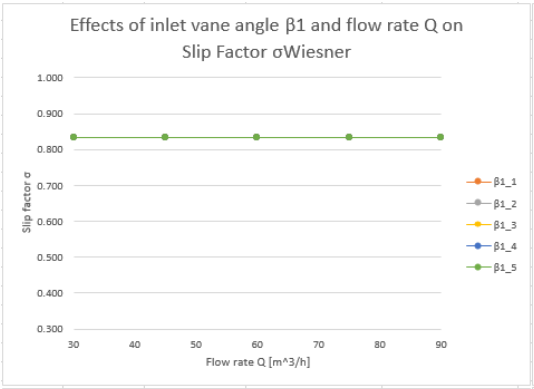

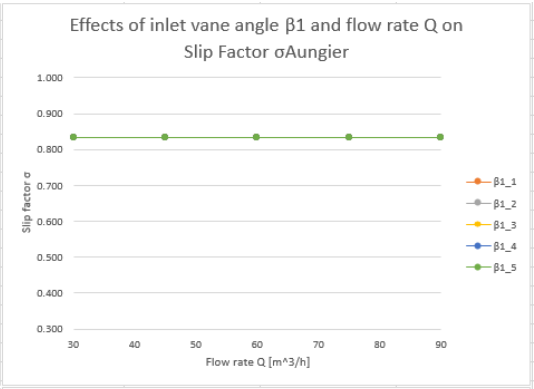

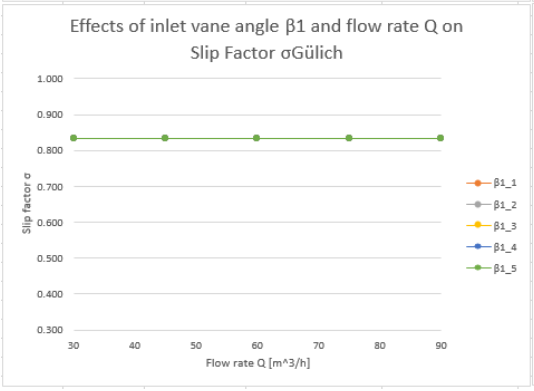

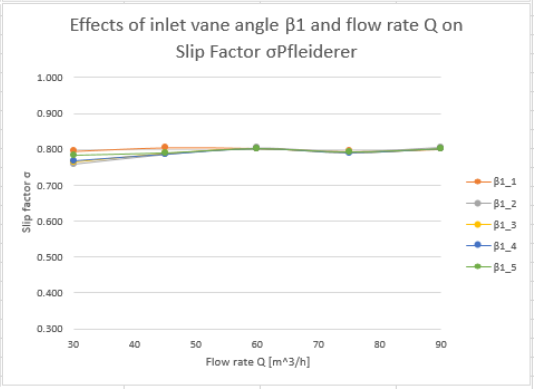

i	1	2	3	4	5
β_{1_i}	8°	10.7°	14°	17°	20°

The results here are rather interesting. The slip factor can increase to ideal flow (σ=1) at high blade angles. Further increase in blade angle will quickly reduce the effect. Change of inlet

vane angles also does contribute very little at high flow rates and has a very significant effect at lower flow rates. None of the models have shown this effect.

9.8 Effects of outlet width on slip factor

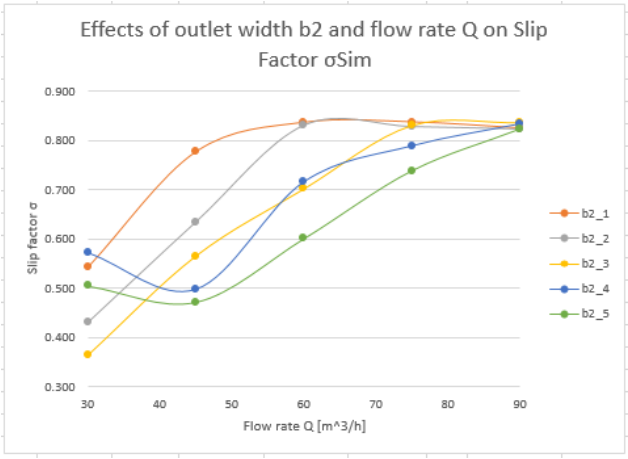

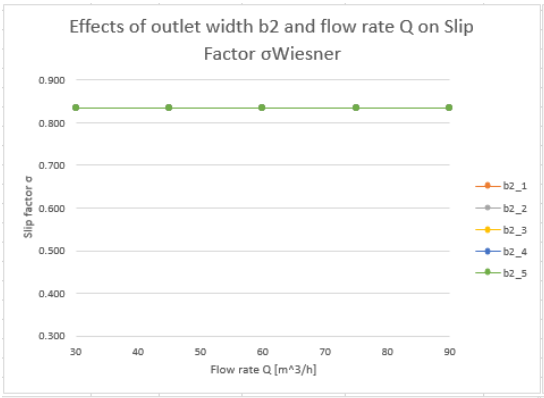

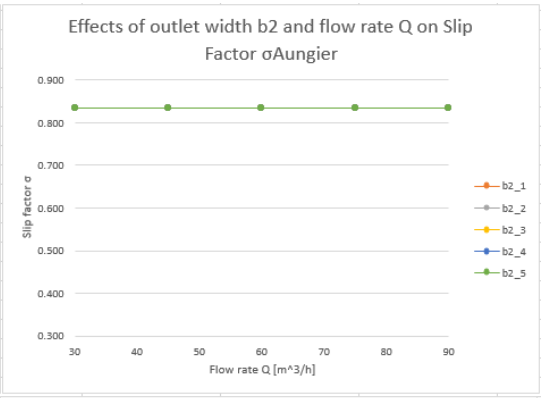

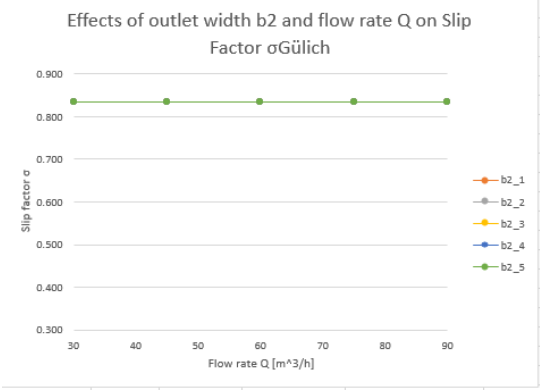

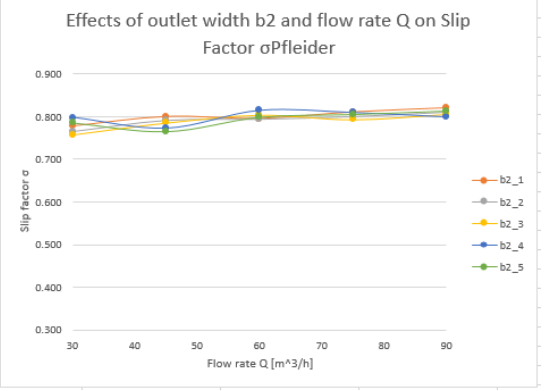

i	1	2	3	4	5
b_{2_i}	$11mm$	$13mm$	$15mm$	$17mm$	$19mm$

Outlet width decrease generally increases slip factor significantly. This is however not the case for very low flow rates. Pfleiderers model again have shown very similar positions of the variables in respect to each other along the range of flow rates.

9.9 Effects of average inlet diameter on slip factor

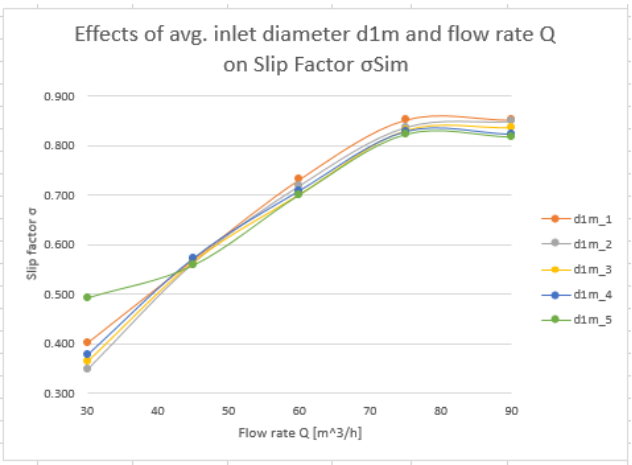

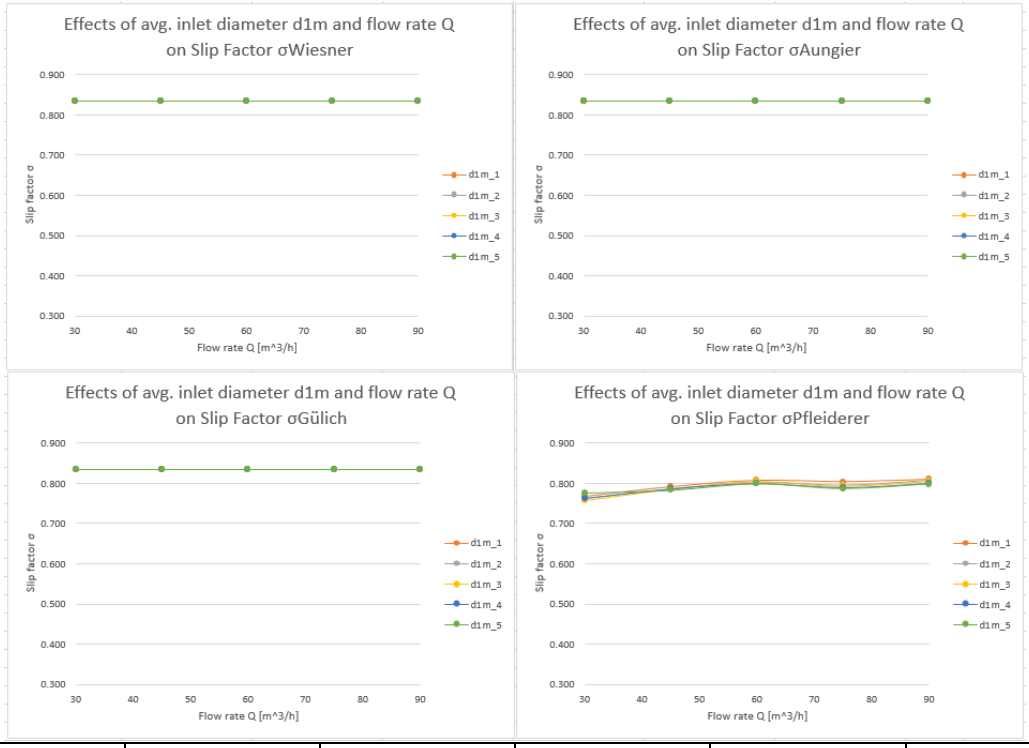

i	1	2	3	4	5
d_{1m_i}	$56.5mm$	$59mm$	$61mm$	$64mm$	$66.5mm$

Inlet diameter of impeller have very little effect in influencing the slip factor as seen on the top figure as well as the four slip factor correlation models.

10 Summary

After evaluating the results, it is found that Wiesners model and its variants from Aungier and Gülich give the most accurate slip factor prediction at high flow rates. Pfleiderer model on the other hand captures the influence of flow rates but only very slightly. More research should be made to create the most accurate model in slip factor correlations. Correlations that have the best accuracy at high flow rates as Wiesner's, as sensitive as Pfleiderers and are more effective in its prediction for flow rates lower than the design point.

11 References

[1] "Centrifugal pumps; denomination and numbering of components," no. DIN 24250 (1984-01-00), p. 51, 1984.

[2] M. A. Bin Zulkifli, *Geometry generation and CFD simulation of radial pump impeller using CFturbo and Star-CCM+*, Coburg: University of Applied Sciences Coburg, 2017.

[3] T. Carolus, Ventilatoren, Siegen: Springer Verlag, 2012.

[4] "www.gempump.com," 2015. [Online]. Available: http://www.gempump.com/project/goulds-3196-impeller/. [Accessed 14 February 2017].

[5] "www.ksb.com," [Online]. Available: https://www.ksb.com/centrifugal-pump-lexicon/impeller/191094/. [Accessed 14 February 2017].

[6] "microtechcastforge.com," 2015. [Online]. Available: http://microtechcastforge.com/investment-casting/products.html. [Accessed 14 February 2017].

[7] "www.businessmagnet.co.uk," Businessmagnet Ltd, 2017. [Online]. Available: http://www.businessmagnet.co.uk/company/gearpumps-67434.htm. [Accessed 14 February 2017].

[8] "www.sulzer.com," [Online]. Available: https://www.sulzer.com/en/Products-and-Services/Pumps-and-Systems/Single-Stage-Pumps/ISO5199-Pumps/Other-ISO5199-Pumps/Process-Pump-BE. [Accessed 14 February 2017].

[9] S. L. Dixon and C. A. Hall, Fluid Mechanics and Thermodynamics of Turbomachinery Seventh Edition, Elsevier Inc., 2014.

[10] P. D.-I. Epple, "Minderleistung in Strömungmaschinen - Entstehung, Zahlenmäßige Beschreibung und Berücksichtigung bei der Auslegung," Coburg, 2016.

[11] C. Pfleiderer and H. Petermann, "Strömungsmaschinen," Springer Verlag, Braunschweig, 2004.

[12] L. C. Team, "Tips & Tricks: Inflation Layer Meshing in ANSYS," 6 January 2012. [Online]. Available: https://www.computationalfluiddynamics.com.au/tips-tricks-inflation-layer-meshing-in-ansys/. [Accessed 21 February 2017].

12 Table of figures

13 List of tables

14 Attachments

Star CCM+ simulation files of the base design of impeller used for this bachelor thesis containing the settings and solutions of the simulation, the different impeller geometries in form of STEP file, as well as the excel sheet used to evaluate the results are provided together with this thesis as attachments in DVD format(s).